

Regge phenomenology of pion photoproduction off the nucleon at forward angles

Byung Geel Yu*

Research Institute of Basic Sciences, Korea Aerospace University, Koyang, 412-791, Korea

Tae Keun Choi†

Department of Physics, Yonsei University, Wonju, 220-710, Korea

W. Kim‡

Department of Physics, Kyungpook National University, Daegu, 702-701, Korea

(Dated: January 13, 2013)

We present a Regge model for pion photoproduction which is basically free of parameters within the framework of the s -channel helicity amplitude. For completeness we take into account axial mesons $a_1(1260)$, $b_1(1235)$ and tensor meson $a_2(1320)$ in addition to the primary $\pi + \rho$ exchanges for charged pion photoproduction, while the axial meson $h_1(1170)$ exchange is added to the model of $\omega + \rho^0 + b_1$ exchanges for the neutral case. The present model deals for the first time with the a_2 and h_1 Regge poles in the s -channel helicity amplitude. For model independence, we use coupling constants of all exchanged mesons determined from empirical decay widths or from the SU(3) relations together with consistency check with existing estimates that are widely accepted in other reaction processes. Based on these coupling constants the simultaneous description of four photoproduction channels is given. Within the Regge regime, $s \gg 4M^2$ and $-t < 2 \text{ GeV}^2$, cross sections and spin polarization asymmetries at various photon energies are analyzed and results are obtained in better agreement with experimental data without referring to any fitting procedure. The model confirms dominance of the nucleon Born term in the sharp rise of the charged pion cross section at very forward angles, while dominance of the ω exchange with the nonsense wrong signature zero leads to the deep dip in the neutral pion cross section. In contrast to existing models, however, our model for the charged pion case shows quite a different production mechanism due to the crucial role of the tensor meson a_2 exchange in the cross section and spin polarization asymmetries. Also the axial meson b_1 exchange is found to give a sizable contribution to the photon polarization asymmetry. In the neutral case, the role of the b_1 is not significant, but the isoscalar h_1 exchange gives an important contribution to the dip-generating mechanism in the photon polarization, showing the isoscalar nature of the process with the ω . These findings demonstrate validity of the present model with the prompt use of the tensor meson a_2 and axial meson h_1 for a wider application.

PACS numbers: 13.40.-f, 13.60.Rj, 13.75.Jz, 13.88.+e

Keywords: Pion photoproduction, Regge pole, s -channel helicity amplitude, Tensor meson, Axial meson

I. INTRODUCTION

For decades progress has been made in both theory and experiment to establish the model for the photoproduction of pseudoscalar mesons from threshold to the resonance region. The effective Lagrangian involving the chiral loop diagram has been applied to realize the aspect of the soft pion dynamics [1], which gradually extends to the intermediate energy region where the low-lying resonance arises from a quasi-bound state of the meson-baryon coupled channel [2, 3]. These models have been developed and tested along with the advent of the experimental facilities, such as the SAPHIR/ELSA, the CLAS/JLab and

the LEPS/SPring-8 [4–8]. But now, however, confronted with on-going plans in these facilities to upgrade the energy scale higher than several tens of GeVs [9], the need for theoretical tools to describe the dynamics of such production mechanisms at high energies that are beyond the scope of the effective Lagrangian approach has grown.

It is known that the Regge formalism can serve to this end with many unknown resonances in the s -channel replaced by the representative t -channel Regge pole by duality [10]. The exchange of the spin quantum number carried by the meson trajectory could provide a most economical way for the description of high-energy phenomenologies [11–19]. In Ref. [13], Kellett considered the $\pi + \rho + a_2$ Regge pole exchanges for the charged pion, and $\omega + \rho + b_1$ exchanges for the neutral case together with their respective cuts in the analysis of high-energy pion photoproduction. He obtained a good fit of all available data on charged and neutral pion cases simultaneously. More recently, Sibirtsev *et al.* repeated the same proce-

*Electronic address: bgyu@kau.ac.kr

†Electronic address: tkchoi@yonsei.ac.kr

‡Electronic address: wooyoung@knu.ac.kr

ture based on an extended version of Ref. [13]. With a global analysis of all world data available, they investigated the applicability of the Regge approach to pion photoproduction in the region $2 \leq \sqrt{s} \leq 3$ GeV, the so-called the fourth resonance region, by extrapolating the cross section at high energy down to the resonance region for comparison [14, 15].

Despite the apparent simplicity, however, these models [13–15] are based on the t -channel helicity amplitude (TCHA) which totally requires a fit. On the other hand, utilizing the photon helicity amplitude specific to the present process [20], Levy, Majerotto and Read (LMR) constructed a model for the $K + K^*$ Regge pole exchanges in the photo and electroproduction of kaon (and $\pi + \rho$ exchanges for the case of pion) [16]. Since the s -channel helicity amplitude (SCHA) of the case is given in terms of the conventional Chew-Goldberger-Low-Nambu (CGLN) amplitude [21] the photoproduction current can be obtained by using the Born approximation for the t -channel exchange of these mesons with the couplings of the meson trajectories to photon or to baryons implemented by the relevant interaction Lagrangians. It is, therefore, advantageous to work with the Regge poles in the SCHA in that one exploits the estimate from the decay width or from the symmetry consideration for the coupling constants of the exchanged meson in the use of the effective Lagrangians. Furthermore, of the photoproduction current, gauge invariance is easily prescribed for the exchange of the pion trajectory by introducing the nucleon Born term, as Guidal, Laget, and Vanderhaeghen (GLV) showed [17]. It turned out that the nucleon Born term could account for the sharp rise of the charged pion cross section at the very forward angle, thus removing the theoretical uncertainty in this region due to the application of the absorptive cut [16] or the parity-doublet conspiring pion [22, 23].

At the present stage, however, the achievements of these models are limited. The numerical consequences in the cross section and spin polarizations show the deficiencies to explain the experimental data at high energy and larger momentum transfer, although the coupling constants of the ρ exchange are taken to be rather strong. In those versions extended to kaon photoproduction [16, 17] this tendency becomes even stronger to give the K^* coupling constants too large values to be realistic. This in turn may disprove that the models of $\pi + \rho$, and of $K + K^*$ exchanges are too simple to be realistic. Meanwhile, the role of the tensor meson exchange, though not yet considered in these models, is found to be of significance as the natural parity exchange in the fit of the Regge poles using the TCHA [13–15].

Motivated by such shortcomings in current model calculations, i.e., the absence of the higher spin exchange and, as a consequence, the poor parametrization of the meson coupling constants, we here investigate the contribution of the higher spin exchange based on the primary

$\pi + \rho$ exchanges to search for the possibility of the Regge approach to pion photoproduction without fit parameters. In the present analysis of the process up to the regime, $-t < 2$ GeV² and $s \gg 4M^2$, we include the exchange of the $a_2(1320)$ meson in the charged pion case with a particular attention to its role dissociated from the leading ρ trajectory. We are also interested in estimating the contribution of the axial meson $h_1(1170)$ to the neutral case, since these are the mesons to be investigated with their roles for the first time in the Regge model utilizing the SCHA. We expect that the result of the present work could provide a reliable base for the study of the resonance as found in recent approaches to photo- and electroproduction processes [18, 19].

This article is organized as follows. In Sec. II we begin with a brief introduction of the SCHA for the present model calculation. An extension of the Regge model follows to include the tensor meson $a_2(1320)$ for the natural parity exchange. For the unnatural parity exchange, we take into account the axial meson $a_1(1260)$ and $b_1(1235)$ exchanges in the charged pion and the $h_1(1170)$ exchange in the neutral pion case. Section III is devoted to the determination of the coupling constant of the exchanged meson prior to application. The radiative decay constant of the exchanged meson is estimated either by using the measured decay width or by the axiomatic meson-dominance hypothesis. The strong coupling constant of the exchanged meson is determined from the SU(3) relation. The numerical results with discussion are presented in the Sec. IV. Three appendices follow with each part containing materials for a more specific discussion.

II. REGGE CONTEXT FOR PION PHOTOPRODUCTION

For the Regge approach to pion photoproduction $\gamma(k) + N(p) \rightarrow \pi(q) + N(p')$ in the SCHA, it is convenient to start with the four positive photon helicity amplitudes defined by Walker [20]

$$\begin{aligned} H_1 &= -\frac{1}{\sqrt{2}} \sin \theta \cos \frac{\theta}{2} (F_3 + F_4), \\ H_2 &= -\frac{2}{\sqrt{2}} \cos \frac{\theta}{2} (F_1 + F_2) + H_3, \\ H_3 &= \frac{1}{\sqrt{2}} \sin \theta \sin \frac{\theta}{2} (F_3 - F_4), \\ H_4 &= \frac{2}{\sqrt{2}} \sin \frac{\theta}{2} (F_1 - F_2) - H_1, \end{aligned} \quad (1)$$

where θ is the production angle between the photon and pion three-momenta. The F_i is the CGLN amplitude defined in the nonrelativistic reduction of the photoproduction amplitude in the center-of-mass frame [21],

$$\frac{\sqrt{MM'}}{4\pi W} \mathcal{M} = F_1 \sigma \cdot \hat{\epsilon} + F_2 i \sigma \cdot \hat{q} \sigma \cdot (\hat{k} \times \hat{\epsilon}) + F_3 \sigma \cdot \hat{k} \hat{q} \cdot \hat{\epsilon} + F_4 \sigma \cdot \hat{q} \hat{q} \cdot \hat{\epsilon}, \quad (2)$$

with the photon polarization vector $\hat{\epsilon}$ and the three-momenta $\hat{k} = \vec{k}/|\vec{k}|$ and $\hat{q} = \vec{q}/|\vec{q}|$ for photon and pion. The W is the invariant energy of the system and the $M(M')$ is the mass of the initial- (final-) state nucleon. The CGLN amplitude F_i is the function of energy and angle θ given by

$$\begin{aligned} F_1 &= C_+ \left[\mathcal{A}_1 + \frac{q \cdot k}{W - M} (\mathcal{A}_3 - \mathcal{A}_4) + (W - M') \mathcal{A}_4 \right], \\ F_2 &= C_- \left[\mathcal{A}_1 - \frac{q \cdot k}{W + M} (\mathcal{A}_3 - \mathcal{A}_4) - (W + M') \mathcal{A}_4 \right], \\ F_3 &= D_+ [(W - M) \mathcal{A}_2 + (\mathcal{A}_3 - \mathcal{A}_4)], \\ F_4 &= D_- [-(W + M) \mathcal{A}_2 + (\mathcal{A}_3 - \mathcal{A}_4)], \end{aligned} \quad (3)$$

with the normalization constants $C_{\pm} = \frac{|\vec{k}|}{4\pi} \sqrt{\frac{E' \pm M'}{2W}}$ and $D_{\pm} = \frac{|\vec{k}||\vec{q}|}{4\pi W} \sqrt{\frac{E' \pm M'}{2W}}$. The $E(E')$ is the initial(final) state nucleon energy. The invariant amplitude \mathcal{A}_i in Eq. (3) is given by the following decomposition of the photoproduction amplitude,

$$\mathcal{M} = \bar{u}'(p') \sum_{i=1}^4 \gamma_5 \mathcal{A}_i M_i u(p) \quad (4)$$

where

$$\begin{aligned} M_1 &= \frac{1}{2}(\not{\epsilon} \not{k} - \not{k} \not{\epsilon}), \\ M_2 &= 2P \cdot k \not{q} \cdot \epsilon - 2P \cdot \epsilon \not{q} \cdot k, \\ M_3 &= q \cdot k \not{\epsilon} - q \cdot \epsilon \not{k}, \\ M_4 &= 2(P \cdot k \not{\epsilon} - P \cdot \epsilon \not{k}) - (M + M') M_1, \end{aligned} \quad (5)$$

are the transition operators with $P = \frac{1}{2}(p + p')$. We use the conventions of Bjorken and Drell [24] through out this work. Note that we adopt the covariant operators, Eq. (5), in the decomposition of the amplitude in order for the t -channel pion pole to be free of the kinematic singularities [25]. (In the case of electroproduction process the decomposition used in Ref. [26] does not guarantee this condition.)

Therefore, the Regge pole exchange in the t -channel is incorporated in the SCHA H_i through the reggeization

of the fixed- t pole in the amplitude \mathcal{M} , which is usually given by the conventional Born terms. The cross section and spin polarization observables formulated in terms of the H_i are presented in Table I. For comparison the definitions of the helicity amplitude used by other authors are collected as well. In the Regge regime, $s \gg 4M^2$ and the small $-t$, the general features of the two different helicity formulations, the TCHA, and the SCHA are discussed in Appendix A.

To express the four channels for charged and neutral pion photoproductions, the invariant amplitude is decomposed into the following form in isospin space:

$$\mathcal{A}_i = \mathcal{A}_i^{(+)} \delta_{a3} + \mathcal{A}_i^{(-)} \frac{1}{2} [\tau_a, \tau_3] + \mathcal{A}_i^{(0)} \tau_a, \quad (6)$$

and the four respective amplitudes for particular physical processes are given by

$$\begin{aligned} \mathcal{A}_i(\gamma p \rightarrow \pi^+ n) &= \sqrt{2}(\mathcal{A}_i^{(0)} + \mathcal{A}_i^{(-)}), \\ \mathcal{A}_i(\gamma n \rightarrow \pi^- p) &= \sqrt{2}(\mathcal{A}_i^{(0)} - \mathcal{A}_i^{(-)}), \\ \mathcal{A}_i(\gamma p \rightarrow \pi^0 p) &= \mathcal{A}_i^{(0)} + \mathcal{A}_i^{(+)}, \\ \mathcal{A}_i(\gamma n \rightarrow \pi^0 n) &= -\mathcal{A}_i^{(0)} + \mathcal{A}_i^{(+)}. \end{aligned} \quad (7)$$

A. Charged pion photoproduction

We now consider the reggeization of the t -channel meson pole on the basis of the Born approximation to the first order approximation of one photon exchange [21]. Following Ref. [17] we introduce the nucleon Born term to restore gauge invariance of the πN system coupling to photon at the tree-level Feynman diagram. We then make a prescription for the reggeization of the t -channel pion exchange by replacing the fixed- t pole with the Regge propagator, while keeping intact the coupling vertices $\gamma\pi\pi$ and πNN given by the effective Lagrangians. Therefore, the reggeized pion pole exchanges are written as

$$\mathcal{M}_{\pi^+} = i\sqrt{2} e g_{\pi NN} \bar{u}'(p') \left[\gamma_5 \frac{(2q - k) \cdot \epsilon}{t - m^2} + \gamma_5 \frac{\not{p} + \not{k} + M}{s - M^2} \left(\not{\epsilon} - \frac{\kappa_p}{2M} \not{\epsilon} \not{k} \right) \right] (t - m^2) \mathcal{P}^\pi(s, t) u(p), \quad (8)$$

$$\mathcal{M}_{\pi^-} = -i\sqrt{2} e g_{\pi NN} \bar{u}'(p') \left[\gamma_5 \frac{(2q - k) \cdot \epsilon}{t - m^2} - \left(\not{\epsilon} - \frac{\kappa_p}{2M} \not{\epsilon} \not{k} \right) \frac{\not{p}' - \not{k} + M'}{u - M'^2} \gamma_5 \right] (t - m^2) \mathcal{P}^\pi(s, t) u(p), \quad (9)$$

TABLE I: Notations for the s -channel helicity amplitudes. (a)[27], (b)[28], and (c)[20]. The net helicity flip is denoted by n . The variable $t = t_{min} - 4|\vec{k}||\vec{q}|\sin^2 \frac{\theta}{2}$, where $t_{min} = (k_0 - q_0)^2 - (|\vec{k}| - |\vec{q}|)^2$.

	Baker ^(a)	Worden ^(b)	Walker ^(c)	Observables of Walker
$n = 0$	N	H_2	H_2	$d\sigma/dt = H_1 ^2 + H_2 ^2 + H_3 ^2 + H_4 ^2$
$n = 1$	S_1	H_4	H_1	$\Sigma d\sigma/dt = 2\text{Re}(H_1^* H_4 - H_2^* H_3)$
$n = 1$	S_2	H_1	H_4	$Td\sigma/dt = 2\text{Im}(H_1^* H_2 - H_3^* H_4)$
$n = 2$	D	H_3	H_3	$Pd\sigma/dt = 2\text{Im}(H_2^* H_4 - H_1^* H_3)$
Normalization	1	$\sqrt{32\pi}(s - M^2)$	$\frac{s - M^2}{\sqrt{2\pi s}}$	

which are gauge invariant for the $\gamma p \rightarrow \pi^+ n$ and $\gamma n \rightarrow \pi^- p$ processes. Here the $g_{\pi NN}$ is the πN strong coupling constant, m is the pion mass, and

$$\mathcal{P}^\pi(s, t) = \frac{\pi\alpha'_\pi}{\Gamma(\alpha_\pi(t) + 1)} \frac{(1 + e^{-i\pi\alpha_\pi(t)})}{2\sin\pi\alpha_\pi(t)} \left(\frac{s}{s_0}\right)^{\alpha_\pi(t)} \quad (10)$$

is the pion Regge propagator, which leads Eqs. (8) and (9) to the usual nucleon and pion Born terms in the limit $t \approx m_\pi^2$, as

$$(t - m^2)\mathcal{P}^\pi(s, t) \rightarrow 1. \quad (11)$$

This on-mass shell relation between the two propagators is easily proved by using the properties of the Γ function [14]. In Fig. 1 the diagrams (a) and (b) show the gauge invariant nucleon and pion Born terms in Eqs. (8) and (9) reggeized through the prescription in Eq. (11). At high energy it is sufficient to neglect the magnetic interaction of the nucleon Born term. In this regard it would be redundant to consider the pseudovector coupling of the πN

interaction which differs from the pseudoscalar coupling one only by the magnetic interaction of the Seagull term.

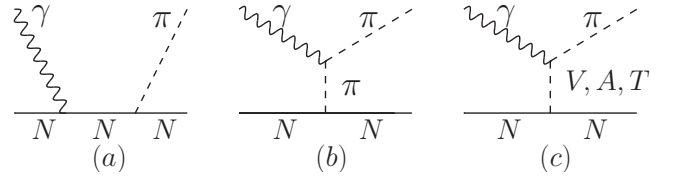


FIG. 1: (Color online) Exchange of t -channel mesons. Diagram (a) is the nucleon Born term and (b) is the pion Regge pole exchange. The diagrams (a) and (b) constitute the gauge invariant pion Regge pole exchange. Diagram (c) represents the vector meson(V), axial vector meson(A), and tensor meson(T) Regge pole exchanges.

The photoproduction amplitudes for the spin-1 vector meson, and axial vector meson exchange are given by

$$\mathcal{M}_V = \frac{g_{\gamma\pi V}}{m_0} \epsilon_{\mu\nu\alpha\beta} \epsilon^\mu k^\nu q^\alpha \frac{(-g^{\beta\rho} + Q^\beta Q^\rho / m_V^2)}{t - m_V^2 + im_V \Gamma_V} \bar{u}'(p') \left[g_{VNN}^v \gamma_\rho + i \frac{g_{VNN}^t}{2M} \sigma_{\lambda\rho} Q^\lambda \right] u(p), \quad (12)$$

$$\mathcal{M}_A = \frac{g_{\gamma\pi A}}{m_0} (k \cdot Q \epsilon_\mu - \epsilon \cdot Q k_\mu) \frac{(-g^{\mu\nu} + Q^\mu Q^\nu / m_A^2)}{t - m_A^2 + im_A \Gamma_A} \bar{u}'(p') \left[g_{ANN}^v \gamma_\nu + i \frac{g_{ANN}^t}{2M} \sigma_{\lambda\nu} Q^\lambda \right] \gamma_5 u(p), \quad (13)$$

respectively, where m_0 is a parameter of mass dimension taken as 1 GeV and $Q = (q - k)$ is the t -channel momentum transfer [29].

The exchange of the tensor meson of spin-2 is given by [30–32]

$$\mathcal{M}_T = \bar{u}'(p') \epsilon_{\alpha\beta\mu\nu} \epsilon^\mu k^\nu q^\alpha q_\rho \frac{\Pi^{\beta\rho;\lambda\sigma}(q - k)}{t - m_T^2 + im_T \Gamma_T} [G_T^{(1)}(\gamma_\lambda P_\sigma + \gamma_\sigma P_\lambda) + G_T^{(2)} P_\lambda P_\sigma] u(p), \quad (14)$$

where the tensor meson coupling constants are

$$G_T^{(1)} = \frac{2g_{\gamma\pi T}}{m_0^2} \frac{2g_{TNN}^{(1)}}{M}, \quad G_T^{(2)} = -\frac{2g_{\gamma\pi T}}{m_0^2} \frac{4g_{TNN}^{(2)}}{M^2}, \quad (15)$$

for brevity and the polarization tensor of the tensor meson is

$$\Pi_{\mu\nu;\rho\sigma}(Q) = \frac{1}{2}(\bar{g}_{\mu\rho}\bar{g}_{\nu\sigma} + \bar{g}_{\mu\sigma}\bar{g}_{\nu\rho}) - \frac{1}{3}\bar{g}_{\mu\nu}\bar{g}_{\rho\sigma},$$

$$(\bar{g}_{\mu\nu} = -g^{\mu\nu} + Q^\mu Q^\nu / m_T^2). \quad (16)$$

These t -channel meson exchanges are depicted in Fig. 1(c). In the above expressions we write collectively the vector meson, $V=\rho(770)(1^+(1^{--}))$, and $\omega(782)(0^-(1^{--}))$ with the isospin and spin quantum number denoted by $I^G(J^{PC})$. For the axial meson, $A=a_1(1260)(1^-(1^{++}))$, $b_1(1235)(1^+(1^{+-}))$, and $h_1(1170)(0^-(1^{+-}))$. The tensor meson $a_2(1320)(1^-(2^{++}))$ is denoted by the T .

With the Regge propagator for the pion exchange given in Eq. (10), the reggeization of the vector meson, axial meson, and the tensor meson exchanges in the photoproduction amplitude follows by replacing each fixed- t pole in Eqs. (12), (13) and (14) with the corresponding Regge propagator of the form

$$\begin{aligned} \mathcal{P}^V(s, t) &= \frac{\pi\alpha'_V}{\Gamma(\alpha_V(t))} \frac{(-1 + e^{-i\pi\alpha_V(t)})}{2 \sin \pi\alpha_V} \left(\frac{s}{s_0}\right)^{\alpha_V(t)-1}, \\ \mathcal{P}^A(s, t) &= \frac{\pi\alpha'_A}{\Gamma(\alpha_A(t))} \frac{(-1 + e^{-i\pi\alpha_A(t)})}{2 \sin \pi\alpha_A} \left(\frac{s}{s_0}\right)^{\alpha_A(t)-1}, \\ \mathcal{P}^T(s, t) &= \frac{\pi\alpha'_T}{\Gamma(\alpha_T(t)-1)} \frac{(1 + e^{-i\pi\alpha_T(t)})}{2 \sin \pi\alpha_T(t)} \left(\frac{s}{s_0}\right)^{\alpha_T(t)-2} \end{aligned} \quad (17)$$

respectively. The scale parameter s_0 is taken as 1 GeV² for the variable (s/s_0) to be dimensionless. The phase factor $\frac{1}{2}(\tau + e^{-i\pi\alpha(t)})$ with the signature $\tau = (-1)^J$ in Eq. (17) is concerned with the notion of the exchange degeneracy (EXD) of ρ - a_2 , or of π - b_1 pair, as discussed in Appendix B.

As to the Regge trajectories of the form, $\alpha(t) = \alpha' t + \alpha_0$, in Eqs. (10) and (17), we have to allow somewhat uncertainties in the choice of the slope α' given in units of GeV⁻² and the intersection α_0 [13, 14, 19, 33]. In this work we use the same ones chosen in Ref. [17] for the primary meson exchanges π , ρ and ω . We take the trajectories of the b_1 and a_2 to be the weakly EXD with π and ρ , respectively. The trajectories of the a_1 and h_1 are chosen to be the same as that of b_1 with their own mass and spin eigenstates specified.

$$\begin{aligned} \alpha_\pi(t) &= 0.7(t - m_\pi^2), \\ \alpha_\rho(t) &= 0.8t + 0.55, \\ \alpha_\omega(t) &= 0.9t + 0.44, \\ \alpha_{a_1}(t) &= 0.7(t - m_{a_1}^2) + 1, \\ \alpha_{b_1}(t) &= 0.7(t - m_{b_1}^2) + 1, \\ \alpha_{h_1}(t) &= 0.7(t - m_{h_1}^2) + 1, \\ \alpha_{a_2}(t) &= 0.8(t - m_{a_2}^2) + 2. \end{aligned} \quad (18)$$

For the charged pion case the vector meson ω , ϕ exchanges and the Pomeron exchange are forbidden by charge conservation. The photoproduction amplitudes are

$$\mathcal{M}_{\pi^+n} = \mathcal{M}_{\pi^+} + \sqrt{2}[\mathcal{M}_{b_1} + \mathcal{M}_{a_1} + \mathcal{M}_\rho + \mathcal{M}_{a_2}] \quad (19)$$

for the $\gamma p \rightarrow \pi^+ n$ process and

$$\mathcal{M}_{\pi^-p} = \mathcal{M}_{\pi^-} + \sqrt{2}[\mathcal{M}_{b_1} - \mathcal{M}_{a_1} + \mathcal{M}_\rho - \mathcal{M}_{a_2}] \quad (20)$$

for the $\gamma n \rightarrow \pi^- p$ process with the π^\pm terms given in Eqs. (8) and (9). The amplitudes for the vector meson, the axial meson, and the tensor meson are given by Eqs. (12), (13), and (14), respectively. The sign of each term follows from the G -parity consideration in the radiative decay vertices $\gamma\pi V$, $\gamma\pi A$, and $\gamma\pi T$ [17]. We now have two options on the condition of each EXD pair, which is either strong or weak. The former condition has been adopted in Refs. [16, 17] to exclude the exchange of b_1 and a_2 . We here opt to choose the weak EXD pair in which case the exchange of the Regge pole in the pair has the coupling vertex different from each other but shares a common phase. Therefore, we take the phases of EXD pairs, π - b_1 and ρ - a_2 as well as the a_1 to be rotating $e^{-i\pi\alpha(t)}$ for the $\gamma p \rightarrow \pi^+ n$ process, whereas the phases of all these meson exchanges are chosen to be constant, 1, for the process $\gamma n \rightarrow \pi^- p$, as explained in Appendix B.

B. Neutral pion photoproduction

The neutral pion photoproduction excludes the nucleon Born term because the t -channel pion exchange is absent from the process by charge conservation. This process is known to allow the one photon exchange in the t -channel through the $\pi^0 \rightarrow \gamma\gamma$ decay known as the Primakoff effect [34, 35]. It could play a role at the very forward angle $-t \approx 0$. Excluding the Primakoff region, we find that neither the two vacuum trajectories P and P' of even parity nor the trajectories associated with the axial meson a_1 and tensor mesons a_2 and f_2 are allowed to decay to $\pi^0\gamma$ by conservation of charge conjugation(C). Therefore, the exchange of the Regge poles for neutral pion photoproduction is composed of the vector mesons ω and ρ , and the axial meson b_1 . In addition, we note that the axial mesons $h_1(1170)$ and $h_1(1380)$, the singlet and octet members of the axial meson nonet to which the b_1 belongs, can also contribute. In consideration of Ref. [36] where the radiative decay width $\gamma\pi h_1(1170)$ was predicted from the coupled channel analysis we find it to be comparable to that of b_1 . We include the axial meson $h_1(1170)$ exchange to contribute as the unnatural parity exchange together with the b_1 . From the isospin relation in Eq. (7) we have

$$\mathcal{M}_{\pi^0 p} = \mathcal{M}_\omega + \mathcal{M}_\rho + \mathcal{M}_{b_1} + \mathcal{M}_{h_1}, \quad (21)$$

$$\mathcal{M}_{\pi^0 n} = \mathcal{M}_\omega - \mathcal{M}_\rho - \mathcal{M}_{b_1} + \mathcal{M}_{h_1}, \quad (22)$$

for the processes $\gamma p \rightarrow \pi^0 p$ and $\gamma n \rightarrow \pi^0 n$, respectively. Since the Regge poles in Eqs. (21) and (22) are not EXD with each other, we take the non-degenerate phase, $\frac{1}{2}(-1 + e^{-i\pi\alpha_\omega})$, for the leading ω trajectory and, in principle, do the same for the rest in both processes. However, we may as well have more freedom to choose the rotating phase $e^{-i\pi\alpha_\rho}$ for the ρ and the constant one for

the axial meson b_1 and h_1 in Eq. (21). In Eq. (22) we also choose the phase of the ω to be non-degenerate, but we take the constant phase for the rest for a better description of the phenomenology as we shall show later.

Before closing this section, it is worth remarking that the discontinuity of the cross section such as a sharp rise or an apparent dip might require a consideration of the Regge cuts arising from the multiple interferences between two or more Regge poles [13, 14, 37–39]. In this work, however, we disregard such higher order effects mainly because we avoid introducing unwanted parameters through the cut. It is, therefore, sufficient to check the consistency of our amplitudes given in Eqs. (19), (20), (21), and (22) with high-energy data in the region, $-t \leq 2 \text{ GeV}^2$ and $s \gg t$.

III. DETERMINATION OF MESON COUPLING CONSTANTS

This section is devoted to the determination of the coupling constants of exchanged mesons by using the axiomatic identities which are based on the vector meson dominance (VMD) for the vector meson and the axial vector meson dominance (AVMD) for axial vector meson coupling to the nucleon, respectively. The validity of the tensor meson dominance (TMD) is discussed for the determination of the tensor meson-nucleon coupling constant. These meson-baryon coupling constants are determined by basically respecting the SU(3) relations. A consistency check of the coupling constants follows by comparing the results with existing estimates that are widely accepted in other reaction processes.

A. Vector meson couplings

For the determination of ρNN coupling constants, we refer to the VMD which assumes the dominance of the ρ^0 in the nucleon electromagnetic form factors coupling to photon [40], i.e.,

$$\langle N | j^\mu(0) | N \rangle = \frac{\langle 0 | j^\mu(0) | \rho \rangle \langle \rho, N | N \rangle}{t - m_\rho^2}, \quad (23)$$

where the nucleon isovector form factors are defined as

$$\langle N | j_a^\mu(0) | N \rangle = \bar{u}(p') [F_1(t) \gamma^\mu + F_2(t) i \sigma^{\mu\nu} q_\nu] \frac{\tau_a}{2} u(p) \quad (24)$$

and t is the four-momentum transfer $q = (p' - p)$ squared. The tensor coupling part vanishes at $q = 0$. The ρ meson decay is given by the current-field identity [41],

$$\langle 0 | j^\mu(0) | \rho \rangle = \frac{m_\rho^2}{f_\rho} \epsilon^\mu. \quad (25)$$

The m_ρ and ϵ^μ are the ρ meson mass and the polarization vector, respectively. The f_ρ is the universal coupling

constant of the ρ meson which is determined by the decay $\rho^0 \rightarrow e^+ e^-$. Therefore, with the ρNN coupling given by

$$\langle \rho, N | N \rangle = g_{\rho NN}^v \bar{u}(p') \gamma^\nu \tau_a u(p) \epsilon_\nu, \quad (26)$$

the VMD in Eq. (23) yields the t -dependence of the isovector form factor

$$\frac{1}{2} F_1(t) = \frac{m_\rho^2}{f_\rho} \frac{1}{m_\rho^2 - t} g_{\rho NN}, \quad (27)$$

which requires at $t = 0$

$$g_{\rho NN}^v = \frac{1}{2} f_\rho. \quad (28)$$

The value for the f_ρ varies in the range from the $f_\rho = 4.94$ estimated from the decay width $\Gamma_{\rho^0 \rightarrow e^+ e^-} = 7.04 \text{ keV}$ to the case of $f_{\rho\pi\pi} = 6.01$ obtained by the width $\Gamma_{\rho^0 \rightarrow \pi^+ \pi^-} = 149.4 \text{ MeV}$. On the other hand, the VMD applied to the low energy s -wave πN scattering leads to $\sqrt{f_{\rho\pi\pi} f_{\rho NN}} = 5.85$. Also there exists an estimate $f_\rho \approx 5.3$ from the empirical analysis of the experimental data on the $N \bar{N} \pi \pi$ [27, 42]. In this work we choose the $f_\rho = 5.2$, rather a moderate one from Refs. [27, 42], and use

$$g_{\rho NN} = 2.6. \quad (29)$$

For the ratio of tensor to vector coupling, κ_ρ , the VMD leads to $\kappa_\rho = 3.7$, whereas $\kappa_\rho \approx 6$ is extracted from the one boson exchange (OBE) analysis of the NN potential [43]. We use $\kappa_\rho = 6.2$ for the present work. For the ωNN coupling constants, we take $g_{\omega NN} = 15.6$ by the ratio $g_\omega = f_\omega = 3f_\rho$ with the tensor coupling ratio $\kappa_\omega \simeq 0$.

The coupling constant of the $\gamma\pi V$ interaction is estimated from the observed decay width. From the effective Lagrangian used in Eq. (12),

$$\mathcal{L}_{\gamma\pi V} = \frac{g_{\gamma\pi V}}{m_0} \epsilon_{\mu\nu\alpha\beta} \partial^\nu \mathcal{A}^\mu \partial^\alpha \pi V^\beta, \quad (30)$$

with the photon field denoted by \mathcal{A} , the decay width is given by,

$$\Gamma_{V \rightarrow \pi\gamma} = \frac{1}{96\pi} \left(\frac{g_{\gamma\pi V}}{m_0} \right)^2 \left(\frac{m_V^2 - m_\pi^2}{m_V} \right)^3, \quad (31)$$

which estimates $g_{\gamma\pi^\pm \rho} = 0.223$ from the measured width $\Gamma_{\rho \rightarrow \gamma\pi^\pm} = 0.068 \text{ GeV}$ and $g_{\gamma\pi^0 \rho} = 0.255$ from the $\Gamma_{\rho \rightarrow \gamma\pi^0} = 0.090 \text{ GeV}$, respectively. These coupling constants are in fair agreement with the prediction of the VMD in the $\omega\rho\pi$ coupling vertex, which states in the manner similar to Eq. (27),

$$g_{\gamma\pi\rho} = e \frac{m_\omega^2}{f_\omega} \frac{1}{m_\omega^2 - t} g_{\omega\rho\pi} \quad (32)$$

with $g_{\omega\rho\pi} = \frac{3f_\rho^2}{8\pi^2 f_\pi} = 11.035 \text{ GeV}^{-1}$ [44] estimated by $f_\rho = 5.2$, $f_\omega = 3f_\rho$, and the pion decay constant $f_\pi = 93.1 \text{ MeV}$.

For $\gamma\pi^0\omega$ coupling, we determine $g_{\gamma\pi^0\omega} = 0.723$ from the empirical decay width $\Gamma_{\omega \rightarrow \gamma\pi^0} = 0.757 \text{ GeV}$, which is comparable to the VMD prediction similar to Eq. (32),

$$g_{\gamma\pi^0\omega} = \frac{e}{f_\rho} g_{\omega\rho\pi}. \quad (33)$$

B. Axial meson couplings

Radiative decays of axial mesons, $A \rightarrow \gamma\pi$, have been investigated in Refs. [45, 46], in which the coupling constants of the mesons were derived from the VMD via the interpolation of the $\rho(\omega)$ meson field into the strong decay $A \rightarrow \rho\pi$ ($A \rightarrow \omega\pi$) for the charged (neutral) meson couplings. Compared with the empirically known cases, predictions by the VMD seem to be reliable, as shown above. Hence we exploit the ω dominance in the decay $b_1 \rightarrow \omega\pi^0$ for the estimate of the $\gamma\pi^0 b_1$ coupling constant the width of which is currently not known. By using the effective Lagrangian for the vector(V)-pseudoscalar meson(φ)-axial meson(A) coupling,

$$\mathcal{L}_{V\varphi A} = \frac{g_{V\varphi A}}{m_0} A^\mu (g_{\mu\nu} q \cdot k - k_\mu q_\nu) V^\nu \varphi, \quad (34)$$

we derive the decay width as in Ref. [46] which estimates $g_{b_1\omega\pi^0} = 9.77$ from the full width $\Gamma_{b_1 \rightarrow \pi\omega} = (142 \pm 9)$ MeV. Thus, we obtain $g_{\gamma\pi^0 b_1} = 0.189$ from the VMD relation,

$$g_{\gamma\pi^0 b_1} = \frac{e}{f_\omega} g_{b_1\omega\pi^0}. \quad (35)$$

For the b_1 decay into the charged pion case the width is reported in the Particle Data Group to be $\Gamma_{b_1 \rightarrow \pi^\pm \gamma} = (0.227 \pm 0.057)$ MeV, and we estimate the coupling constant to be $g_{\gamma\pi^\pm b_1} = 0.196$ by use of Eq. (31). These values are comparable with the chiral-unitary model predictions, $g_{\gamma\pi^\pm b_1} = 0.187$, and $g_{\gamma\pi^0 b_1} = 0.173$ [36]. The empirical information on the decays of the isoscalar $h_1(1170)$ and $h_1(1380)$ mesons is very scarce. We refer to the chiral-unitary model predictions for the decay widths $\Gamma_{h_1(1170) \rightarrow \pi^0 \gamma} = 837 \pm 134$ keV and $\Gamma_{h_1(1380) \rightarrow \pi^0 \gamma} = 81 \pm 18$ keV, which yield $g_{\gamma\pi^0 h_1(1170)} = 0.405$ and $g_{\gamma\pi^0 h_1(1380)} = 0.098$, respectively. Thus the $h_1(1380)$ exchange is neglected for the small coupling constant hereafter.

The case of determining the $g_{\gamma\pi a_1}$ coupling constant is somewhat uncertain, because only the full width is given in a broad range, $\Gamma = 250 \sim 600$ MeV. Therefore, even if we use the VMD to estimate the coupling constant, as before,

$$g_{\gamma\pi^\pm a_1} = \frac{e}{f_\rho} g_{\rho\pi^\pm a_1}, \quad (36)$$

we still need to know the partial decay width $\Gamma_{a_1 \rightarrow \pi\rho}$ for the determination of the $g_{\rho\pi^\pm a_1}$. For this reason Xiong [45] and Haglin [46] assumed the width $\Gamma_{a_1 \rightarrow \pi\rho} = 400$ MeV to obtain $g_{\gamma\pi^\pm a_1} = 0.743$. We find, however, that this value yields the partial width $\Gamma_{a_1 \rightarrow \pi\gamma} = 1.4$ MeV, which certainly overestimates the experimental value 0.64 ± 0.246 MeV [47–49]. In this work we choose the $\Gamma_{a_1 \rightarrow \gamma\pi} = 0.64$ MeV to estimate $g_{\gamma\pi^\pm a_1} = 0.316$, which corresponds to the width $\Gamma_{a_1 \rightarrow \pi\rho} \approx 250$ MeV. This choice is reasonable, as compared to the chiral unitary model estimate where the decay width was predicted to

be $\Gamma_{a_1 \rightarrow \pi\gamma} = 0.46 \pm 0.1$ MeV, and $g_{\gamma\pi a_1} = 0.268$, as a result [36]. We note that this value is within the range of the widths 0.630 ± 0.246 MeV.

For the determination of the axial meson coupling constants, g_{ANN}^v , and g_{ANN}^t in Eq. (13), we apply the AVMD to the nucleon axial form factors [50, 51]

$$\langle N | j_5^\mu(0) | N \rangle = \bar{u}(p') [F_A(t) \gamma^\mu + F_T(t) i \sigma^{\mu\nu} q_\nu] \gamma_5 \frac{\tau_a}{2} u(p) \quad (37)$$

where $F_A(t)$ is the axial vector form factor with $F_A(0) = g_A$, and $F_T(t)$ is the pseudotensor one. The induced pseudoscalar form factor $F_P(t) q^\mu \gamma_5$ is omitted here for irrelevance. Since the nucleon axial vector vertex $\gamma^\mu \gamma_5$ is C -even and the pseudotensor coupling vertex $\sigma^{\mu\nu} \gamma_5$ is C -odd, the a_1 meson of C -even couples to the nucleon via the axial vector coupling only, whereas both the b_1 and h_1 mesons of C -odd couple to the nucleon axial current with the pseudotensor coupling, but not with the axial vector coupling [19].

1. a_1 vector coupling constant

In analogy to the ρ meson dominance as before, the nucleon axial vector current is assumed to be dominated by the a_1 -pole, and this idea is known to hold up to the momentum transfer $t \approx 1$ GeV² for the optimal fit of the axial form factor $F_A(t)$ to experimental data [52]. Thus, the matrix element of the nucleon axial vector current is

$$\langle N | j_5^\mu(0) | N \rangle = \frac{\langle 0 | j_5^\mu(0) | a_1 \rangle \langle a_1 | N \rangle}{t - m_{a_1}^2}. \quad (38)$$

The charged a_1 meson decay to vacuum through the axial vector current is given by

$$\langle 0 | j_5^\mu(0) | a_1 \rangle = \frac{f_{a_1}}{\sqrt{2}} \epsilon^\mu, \quad (39)$$

where the a_1 decay constant $f_{a_1} = (0.19 \pm 0.03)$ GeV² is measured from the $\tau^- \rightarrow a_1^- + \nu_\tau$ decay process. The a_1 coupling to nucleon is given by

$$\langle a_1 | N \rangle = g_{a_1 NN}^v \bar{u}(p') \gamma^\nu \gamma_5 \tau_a u(p) \epsilon_\nu. \quad (40)$$

Then, we obtain the relation between the axial vector form factor and the strong coupling vertex of the axial meson at $t = 0$ in Eq. (38) [50],

$$g_{a_1 NN}^v = \frac{1}{2} \frac{\sqrt{2} m_{a_1}^2}{f_{a_1}} g_A. \quad (41)$$

We are now able to determine $g_{a_1 NN}^v$ with the nucleon axial charge $g_A = 1.25$. But the EMC experiment reported rather a smaller value,

$$g_A = (\Delta u - \Delta d) = 1.134, \quad (42)$$

measured in terms of the quark helicity Δq involving the sea quarks and gluon contributions. This leads to

$$g_{a_1 NN}^v = 6.7, \quad (43)$$

and we find it to be in agreement with the $g_{a_1 NN}^2/4\pi = 3.3$ extracted from the analysis of NN interaction [53].

2. b_1 & h_1 tensor coupling constant

In order to determine the tensor coupling constants of the $b_1 NN$ and $h_1 NN$ interactions, we apply the AVMD to the nucleon pseudotensor form factor,

$$\langle N | j_5^{\mu\nu}(0) | N \rangle = \sum_{A=b_1, h_1} \frac{\langle 0 | j_5^{\mu\nu}(0) | A \rangle \langle A, N | N \rangle}{m_A^2 - t} \quad (44)$$

with the pole dominance in Eq. (44) allowed for the b_1 and h_1 , as discussed. The axial meson decay via the pseudotensor current is written as

$$\langle 0 | j_5^{\mu\nu}(0) | A \rangle = i f_A (\epsilon^\mu q^\nu - \epsilon^\nu q^\mu), \quad (45)$$

with the axial meson decay constant f_A . The decay constants are taken as $f_{b_1} = \frac{\sqrt{2}}{m_{b_1}} f_{a_1} \simeq 0.21$ GeV and $f_{h_1} = f_{b_1}$ [51]. The strong coupling of the axial meson to the nucleon pseudotensor current is given by

$$\langle A, N | N \rangle = \frac{g_{ANN}^t}{2M} \bar{u}(p, s_T) i \sigma^{\alpha\beta} \gamma_5 q_\beta \epsilon_\alpha \tau_a u(p, s_T) \quad (46)$$

and we identify the nucleon pseudotensor form factor in Eq. (44) with the matrix element of the bilinear quark tensor current [51],

$$\begin{aligned} \langle N(p, s_T) | \bar{q}_a \sigma^{\mu\nu} \gamma_5 \frac{\lambda_a}{2} q_a | N(p, s_T) \rangle \\ = 2 \delta q^a(\mu^2) (p^\mu s_T^\nu - p^\nu s_T^\mu), \end{aligned} \quad (47)$$

where $J_{5a}^{\mu\nu} = \bar{q}_a \sigma^{\mu\nu} \gamma_5 \frac{\lambda_a}{2} q_a$ and the q_a denotes the quark field of flavor $a = u, d, s$. $N(p, s_T)$ is a nucleon state of momentum p and spin transversity s_T [54]. The δq^a is the quark transversity which counts the valence quarks of opposite transversities in the transversely polarized nucleon. The measurement of the δq^a depends on the renormalization point μ^2 , since the chiral-odd pseudotensor current given in Eq. (47) is not conserved. Thus, in contrast to the axial charge, the nucleon tensor charge is determined by the quark transversity δq^a measured at the renormalization point μ^2 in Eq. (47).

Combining the above ingredients with each other in Eq. (44), we obtain [51]

$$\begin{aligned} g_{b_1 NN}^t &= (\delta u - \delta d) \frac{\sqrt{2} m_{b_1}^2 M}{f_{b_1} < q_\perp^2 >}, \\ g_{h_1 NN}^t &= (\delta u + \delta d) \frac{\sqrt{2} m_{h_1}^2 M}{f_{h_1} < q_\perp^2 >}, \end{aligned} \quad (48)$$

where the $< q_\perp^2 >$ is the quark transverse momentum squared inside the nucleon. We, therefore, determine the tensor coupling constant of the axial meson from the knowledge of the quark transversity δq^a and the quark transverse momentum together with the decay constants given above. According to Ref. [51] the quark transverse momentum squared in Eq. (48) is found to vary within the range, $< q_\perp^2 > \simeq 0.58 \sim 1.0$ GeV², inside the

nucleon. Hence, the present approach to the estimate of the g_{ANN}^t must allow the uncertainty depending on the intrinsic quark momentum as well as the renormalization point of the quark transversity. Furthermore, as the precise measurement of these latter quantities are still in progress, the application of the AVMD to the nucleon axial tensor form factor might be in question. However, as we shall show in Table II below, our estimate for the coupling constant $g_{b_1 NN}^t (g_{h_1 NN}^t)$ from Eq. (48) is valid within the range of the nucleon axial tensor charge predicted by various QCD-inspired models.

As to the estimate of the δq^a the model-independent inequalities, though approximated, are known to be $|\delta u| < 3/2$ and $|\delta d| < 1/3$ [55]. There also exist scattered values for the δq^a from various model calculations depending on what renormalization point they adopted [56–58]. Table II summarizes existing estimates for the δq^a and the g_{ANN}^t as a result. We choose the δq^a from the light cone model [64] in estimating the g_{ANN}^t with signs in Table IV favorable to reproduce the photoproduction data within the range, because the quark helicities Δu and Δd from the model lead to the closest value for the nucleon axial charge $g_A = 1.25$ [65].

It should be noted that our viewpoint in Eq. (48) is opposite to Ref. [51]; To be consistent with Eq. (13) we identify the interaction vertex in Eq. (46) with the tensor coupling constant g_{ANN}^t , and determine it by using currently known values of the δq^a based on the QCD-inspired models. On the contrary the authors of Ref. [51] used the known coupling constant g_{ANN} in Eq. (46) (which was determined from the SU(3) relation with the $g_{a_1 NN}^v$), and consequently in Eq. (48), in order to estimate the unknown δq^a .

C. Tensor meson couplings

Since the radiative decay $a_2 \rightarrow \gamma\pi$ is empirically known with its width $\Gamma_{a_2 \rightarrow \pi\gamma} = (0.287 \pm 0.03)$ MeV reported in the Particle Data Group, we estimate the coupling constant for the interaction $\gamma\pi T$ by using the effective Lagrangian [30]

$$\mathcal{L}_{\gamma\pi T} = -i \frac{g_{\gamma\pi T}}{m_0^2} \tilde{F}_{\alpha\beta} (\partial^\alpha T^{\beta\rho} - \partial^\beta T^{\alpha\rho}) \partial_\rho \pi + \text{H.c.} \quad (49)$$

where $\tilde{F}_{\alpha\beta} = \frac{1}{2} \epsilon_{\alpha\beta\mu\nu} F^{\mu\nu}$ is the pseudotensor photon field and the $T^{\alpha\rho}$ is the tensor meson field, a_2 . From the Lagrangian in Eq. (49), the decay width is given by [30]

$$\Gamma_{a_2 \rightarrow \pi\gamma} = \frac{1}{10\pi} \left(\frac{g_{\gamma\pi a_2}}{m_0^2} \right)^2 \left(\frac{m_{a_2}^2 - m_\pi^2}{2m_{a_2}} \right)^5, \quad (50)$$

and we obtain $g_{\gamma\pi a_2} = 0.276$.

It is of importance to determine the TNN coupling constant on the firm ground. This is, however, not an easy task, not only because information necessary for this is scarce but also because existing estimates for this are rather diverse in both sides of theoretical and experiment

TABLE II: Tensor coupling constants of axial mesons from quark transversities within the range $\langle q_\perp^2 \rangle = 0.58 \sim 1.0 \text{ GeV}^2$. Model predictions for the quark transversity are quoted from Ref. [51]. References are from the lattice [58], QCD sum rule [56], MIT bag model [59], constituent quark model [60], quark soliton model [57, 61], NJL model [62, 63], and light cone calculation [64].

	Lattice	QCD sum rule	Bag	Constituent QM	Quark Soliton	NJL	LC
δu	0.84	1.33	1.09	1.17	1.07	0.82	1.17
δd	-0.23	0.04	-0.27	-0.26	-0.38	-0.07	-0.29
$g_{b_1 NN}^t$	10.31~17.77	12.43~21.43	13.1~22.59	13.78~23.75	13.97~24.08	8.58~14.78	14.07~24.25
$g_{h_1 NN}^t$	5.28~9.1	11.85~20.43	7.09~12.23	7.87~13.57	5.96~10.29	6.49~11.18	7.61~13.12

studies. Therefore, as a guidance to figure out the TNN coupling constant, we first attempt to use the TMD hypothesis in the hadron energy-momentum tensor form factors.

With an assumption of the $f_2(1270)$ -pole dominance in the nucleon and pion energy-momentum tensor form factors, $\langle N | \Theta^{\mu\nu} | N \rangle$ and $\langle \pi | \Theta^{\mu\nu} | \pi \rangle$, respectively [32, 66], the effective Lagrangian for the TNN coupling

$$\mathcal{L}_{TNN} = -2i \frac{g_{TNN}^{(1)}}{M} \bar{N} (\gamma_\lambda \partial_\sigma + \gamma_\sigma \partial_\lambda) N T^{\lambda\sigma} + 4 \frac{g_{TNN}^{(2)}}{M^2} \partial_\lambda \bar{N} \partial_\sigma N T^{\lambda\sigma}, \quad (51)$$

leads to the following identity,

$$\frac{2}{M} (g_{f_2 NN}^{(1)} + g_{f_2 NN}^{(2)}) = \frac{g_{f_2 \pi\pi}}{m_f}. \quad (52)$$

Details in the derivation of Eq. (52) and the relevant $\mathcal{L}_{T\pi\pi}$ are given in Appendix C. Thus, the TMD enables us to determine $g_{f_2 NN}^{(1)} = \pm 2.18$ with $g_{f_2 \pi\pi} = \pm 5.9$ estimated from the decay width $\Gamma_{f_2 \rightarrow \pi\pi} = 156.9_{-1.2}^{+3.8} \text{ MeV}$, as $g_{f_2 NN}^{(2)} \approx 0$ chosen by the normalization conditions of the one-nucleon state with mass, and spin, respectively. [31, 32, 67]. In a similar way, we obtain $g_{a_2 NN}^{(1)} = \pm 2.43$ and $g_{a_2 NN}^{(2)} = 0$ with $g_{a_2 KK} = \pm 6.83$ taken from the observed decay width $\Gamma_{a_2 \rightarrow K\bar{K}} = (5.3 \pm 0.25) \text{ MeV}$ [30]. But we also note that these predictions by the TMD are widely different from those found in phenomenological studies of meson-, and photon-induced reactions. Engles derived estimates of $g_{f_2 NN}^{(1)} = 6.45$ and $g_{f_2 NN}^{(2)} \approx 0$ from the backward πN dispersion relations [68]. Kleinert and Weisz determined $g_{a_2 NN}^{(1)} = 1.54$ and $g_{a_2 NN}^{(1)} \approx -g_{a_2 NN}^{(2)}$ from the dispersion relations for pion photoproduction at threshold [31]. (Our coupling constants are related to Refs. [31, 68] by $g_{f_2 NN}^{(1,2)} = G_{f_2 NN}^{(1,2)}/4$ in Eq. (51)) These values for the $f_2 NN$ and $a_2 NN$ couplings were found to be consistent with those from the detailed analysis of the Compton scattering $\gamma N \rightarrow \gamma N$ [69]. Unlike the VMD and AVMD, therefore, it is not clear whether the application of the TMD is effective for the determination of the coupling constant $a_2 NN$, and $f_2 NN$ as well. This point was discussed in Ref. [66], where various versions of the TMD were examined to conclude that such

an assumption of the pure f_2 -pole dominance as in Eq. (52) may not be correct and that the proper use of the TMD would require further contribution including an additional isoscalar piece in the trace Θ_μ^μ , which is much more involved in the violation of the scale invariance, i.e., probably dilaton [70], or Pomeron [66] as a possible candidate. Hence, we regard that, though a viable hypothesis analogous to the VMD, the validity of the TMD within the simple pole description is questionable and needs further test [71].

We now proceed to determine the tensor meson coupling constants from those found in phenomenological analyses, while keeping the SU(3) symmetry as a good approximation to the tensor meson nonet coupling to the baryon octet [12]. For a reliable choice, we refer to consistency check of the SU(3) relation between the $a_2 NN$ and the $f_2 NN$ couplings,

$$g_{f_2 NN}^{(1)} = \frac{1}{\sqrt{3}} (4\alpha - 1) g_{a_2 NN}^{(1)}, \quad (53)$$

while we let $g_{f_2 NN}^{(2)} \approx 0$, and $g_{a_2 NN}^{(2)} \approx 0$, as before. The couplings of the tensor meson nonet trajectories to the baryons had been investigated to test the SU(3) symmetry for the residues of the tensor meson nonet, and there, the ratio $F/D = -1.8 \pm 0.2$ was estimated to agree with that obtained from high energy experiments [72, 73]. Adopting the ratio in Eq. (53) with the $g_{f_2 NN}^{(1)}$ taken from typical models discussed above, we present the SU(3) predictions for the coupling constant of the $a_2 NN$ in Table III.

Accordingly, we find that the values $g_{f_2 NN}^{(1)} = 6.45$ and $g_{a_2 NN}^{(1)} = 1.54$ determined in Refs. [31, 69] are in good

TABLE III: SU(3) predictions for the coupling constant of the tensor meson a_2 from existing estimates of the f_2 coupling constant. The value of $g_{f_2 NN}^{(1)}$ is taken from other references as per alphabetical superscript ^aRef. [66], ^bRef. [74], ^cRefs. [32, 75], and ^dRef. [68] in order.

	TMD	A	B	C	$(\frac{F}{D})_{\text{exp}} = -1.8 \pm 0.2$
$g_{f_2 NN}^{(1)}$	2.18 ^a	3.38 ^b	5.26 ^c	6.45 ^d	
$g_{a_2 NN}^{(1)}$	0.39	0.6	0.94	1.15	$\alpha = 2.67, \frac{F}{D} = -1.6$
$g_{a_2 NN}^{(1)}$	0.47	0.73	1.14	1.4	$\alpha = 2.25, \frac{F}{D} = -1.8$
$g_{a_2 NN}^{(1)}$	0.54	0.84	1.3	1.6	$\alpha = 2.0, \frac{F}{D} = -2.0$

agreement with the SU(3) predictions with the case of $\alpha = 2.25$ or $\alpha = 2.0$ in column C of Table III. Furthermore these values are also supported by the value $g_{a_2 NN}^{(1)} = 1.57$ extracted from the Nijmegen soft-core YN potential [76, 77] and its extended version [78]. In this work we favor to choose the SU(3) values $g_{a_2 NN}^{(1)} = 1.4$ and $g_{a_2 NN}^{(2)} \approx 0$ from Table III as a median value for the present calculation. We consider that the results should be valid to what extent the symmetry is a good approximation to the couplings of the tensor meson nonet to baryons. In the next section we calculate differential cross section and spin polarizations using $g_{a_2 NN}^{(1)} = 1.4$ and $g_{a_2 NN}^{(2)} = 0$. But we also consider the case of $g_{a_2 NN}^{(2)} \approx -g_{a_2 NN}^{(1)}$ by taking $g_{a_2 NN}^{(2)} = -1.2$ [69] for an exploratory study and show that numerical evidences support the choice $g_{a_2 NN}^{(2)} = 0$ rather than $g_{a_2 NN}^{(2)} \approx -g_{a_2 NN}^{(1)}$ in the analysis of these observables.

IV. RESULTS AND DISCUSSION

In this section we present the numerical results of the four photoproduction processes, $\gamma p \rightarrow \pi^+ n$, $\gamma n \rightarrow \pi^- p$, $\gamma p \rightarrow \pi^0 p$ and $\gamma n \rightarrow \pi^0 n$, with the coupling constants chosen in Table IV.

A. Charged pion photoproduction

1. Differential cross section

The dynamical feature of the charged pion process is characterized by the sharp rise at the very forward angle $-t \leq m_\pi^2$ in the differential cross section as well as the spin polarization asymmetry.

Figure 2 shows the forward angle differential cross sections for the $\gamma p \rightarrow \pi^+ n$ process at five photon energies $E_\gamma = 3.5, 5, 8, 11$ and 16 GeV. The solid curve results from the present work. The cross section is not sensitive to the choice between $g_{a_2 NN}^{(2)} = 0$ and $g_{a_2 NN}^{(2)} = -1.2$ as shown. As the unnatural parity exchange, the contribution of the axial meson is found insignificant in the

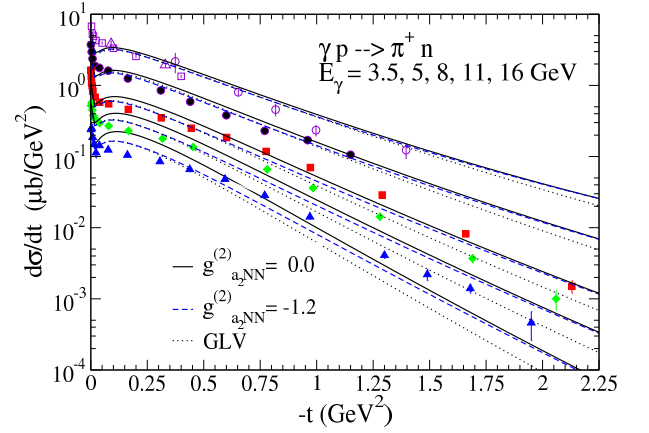


FIG. 2: (Color online) Differential cross sections for $\gamma p \rightarrow \pi^+ n$ at photon energies $E_\gamma = 3.5, 5, 8, 11$, and 16 GeV, respectively. Solid curves result from the gauge invariant $(\pi + b_1) + a_1 + (\rho + a_2)$ exchanges with $g_{a_2 NN}^{(1)} = +1.4$ and $g_{a_2 NN}^{(2)} = 0$, while dashed ones (blue) from $g_{a_2 NN}^{(1)} = +1.4$ and $g_{a_2 NN}^{(2)} = -1.2$. Dotted curves result from the GLV model with the gauge invariant $\pi + \rho$ exchanges. The data are taken from Refs. [85] (open squares), [86] (open triangles), [87] (open circles) and [88] (filled circles, filled squares, filled diamonds and filled triangles).

differential cross section. Compared to the GLV model (the dotted curve), it is clear that the exchange of the a_2 in the present model makes improved the t -dependence of the cross section as the energy and the momentum transfer $-t$ increase. The forward peaks near $|t| \approx m_\pi^2$ are reproduced in Fig. 3 to show the role of the nucleon Born term in this region. In order for the clear differentiation between the model prediction with and without the a_2 exchange, we present Fig. 4 for future experimental test.

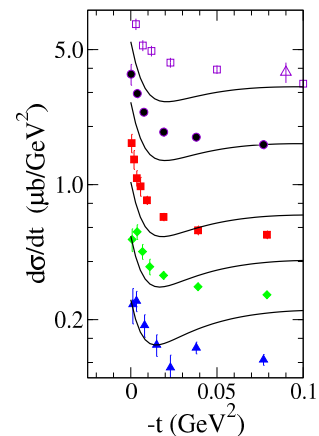


FIG. 3: (Color online) Forward peaks in the region $|t| \approx m_\pi^2$ magnified from Fig. 2 with the same notation for the solid curve.

In Fig. 5 the contribution of each meson exchange to the cross section is displayed for the $\gamma p \rightarrow \pi^+ n$ process

TABLE IV: Coupling constants of exchanged mesons. Radiative decay widths are given in units of keV. The values in the models, LMR(including the multiplicative factor $\lambda = 2.18$), GLV, KM [19], and NSC [76] are taken from the Regge approach. The values for NN/YN [79–81], ESC04 [82], and ESC04₉₇ [83, 84] are extracted from the one boson exchange potentials. The decay width in the parenthesis is the prediction by the chiral unitary model [36].

	LMR	GLV	KM	NSC	NN/YN	ESC04	ESC04 ₉₇	Present work	$\Gamma(\text{keV})$
$g_{\pi NN}/\sqrt{4\pi}$	3.82	3.81	3.78	3.7	3.66	3.58		3.78	
$g_{\gamma\pi^\pm\rho}$		0.224	0.22					0.224	68 ± 7
$g_{\gamma\pi^0\rho}$		0.224						0.255	90 ± 12
$g_{\rho NN}^v$	2.8	3.4	3.4	3.16	2.11	2.77	2.967	2.6	
$g_{\rho NN}^t$	$\kappa_\rho=14.6$	$\kappa_\rho=6.1$	6.1	13.338	17.08	12.31	12.52	$\kappa_\rho=6.2$	
$g_{\gamma\pi^0\omega}$		0.687						0.723	757 ± 27
$g_{\omega NN}^v$		15		10.446	11.96	10.683	10.36	15.6	
$g_{\omega NN}^t$		0		3.224	8.3	1.583	4.2	0	
$g_{\gamma\pi^\pm b_1}$		0.187	0.195					0.196	230 ± 60
$g_{\gamma\pi^0 b_1}$		$\sqrt{2}g_{\gamma\pi^\pm b_1}$						0.189	VMD
$g_{b_1 NN}^v$		16.44				10.96		-	
$g_{b_1 NN}^t$		0	≥ 7.1					-14	
$g_{\gamma\pi^\pm a_1}$			0.33					0.316	640 ± 246
$g_{a_1 NN}^v$			7.1			9.014		6.7	
$g_{\gamma\pi^0 h_1}$								0.405	(837 ± 134)
$g_{h_1 NN}^t$								-9	
$g_{\gamma\pi^\pm a_2}$								0.276	287 ± 30
$g_{a_2 NN}^{(1)}$				1.573				1.4	
$g_{a_2 NN}^{(2)}$								0	

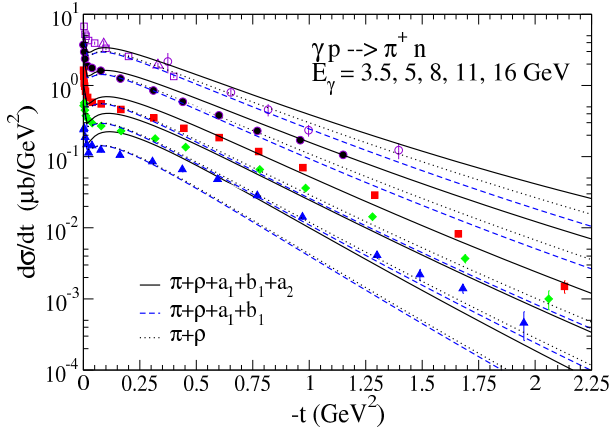


FIG. 4: (Color online) Role of the tensor meson a_2 Regge pole in the differential cross section for $\gamma p \rightarrow \pi^+ n$. The solid line is our model prediction from the $(\pi + b_1) + a_1 + (\rho + a_2)$ exchanges with $g_{a_2 NN}^{(1)}(g_{a_2 NN}^{(2)}) = 1.4(0)$, and the blue dashed line is from $\pi + b_1 + a_1 + \rho$. The dotted line is from the primary $\pi + \rho$ exchanges.

at $E_\gamma = 5$ GeV. The pion exchange gives the leading contribution as depicted by the long dashed line. The a_2 exchange with $g_{a_2 NN}^{(1)} = 1.4$ and $g_{a_2 NN}^{(2)} = 0$ gives the contribution comparable to that of the ρ exchange, both of which are smaller than the pion exchange by an order

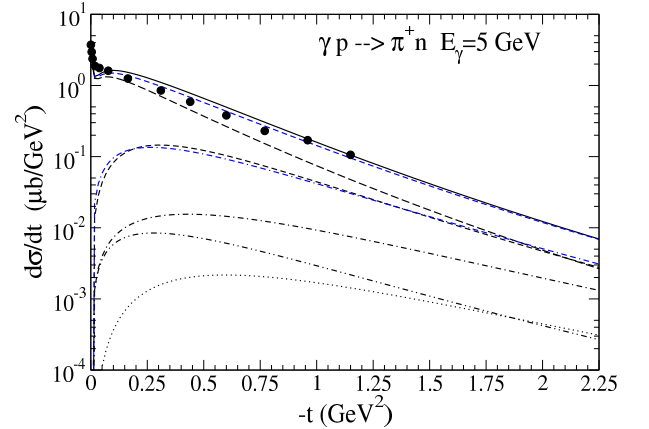


FIG. 5: (Color online) Contribution of each meson exchange to the differential cross section for $\gamma p \rightarrow \pi^+ n$ at $E_\gamma = 5$ GeV. The solid line is our model prediction from the $(\pi + b_1) + a_1 + (\rho + a_2)$ exchanges with $g_{a_2 NN}^{(1)}(g_{a_2 NN}^{(2)}) = 1.4(0)$, and the corresponding one with the $g_{a_2 NN}^{(1)}(g_{a_2 NN}^{(2)}) = 1.4(-1.2)$ is given by the dashed line(blue). The long dashed line(black) is from π exchange. The short dashed line(black) is from the ρ exchange. The dash-dash-dotted line(blue) is from the a_2 exchange with $g_{a_2 NN}^{(1)}(g_{a_2 NN}^{(2)}) = 1.4(0)$, and the dash-dotted line is from the a_2 exchange with $g_{a_2 NN}^{(1)}(g_{a_2 NN}^{(2)}) = 1.4(-1.2)$. The dot-dot-dashed line is from a_1 exchange, and the dotted line from b_1 exchange.

of magnitude. However, the case of $g_{a_2 NN}^{(2)} = -1.2$ falls off the a_2 contribution to be nearly the same contribution of a_1 , which is smaller than the pion exchange by two orders of magnitude.

We present the differential cross section for the $\gamma n \rightarrow \pi^- p$ process at $E_\gamma = 3.4$ GeV in Fig. 6. The constant phase for all exchanged mesons required by the EXD is consistent with data, as discussed in Eq. (20). Each meson exchange gives the same contribution as the case of the $\gamma p \rightarrow \pi^+ n$ process, but with the opposite signs in the π , a_1 and a_2 exchanges by the G parity argument.

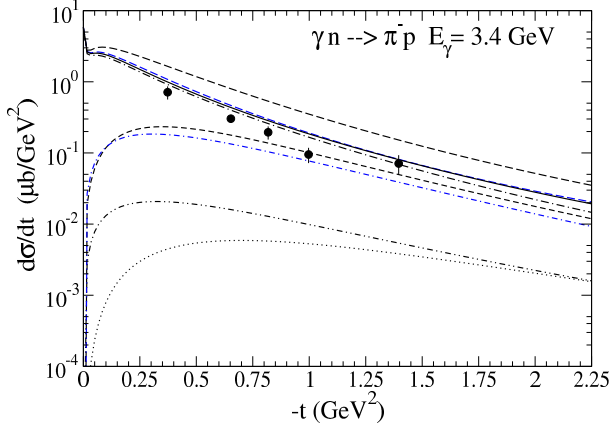


FIG. 6: (color online) Differential cross section for $\gamma n \rightarrow \pi^- p$ at $E_\gamma = 3.4$ GeV. Notations are the same as in Fig. 5 except for the dot-dashed line from the GLV model calculation. For the given $g_{a_2 NN}^{(1)} = 1.4$, the solid line results from the $(-\pi + b_1) - a_1 + (\rho - a_2)$ exchanges with $g_{a_2 NN}^{(2)} = 0$, while the dashed one(blue) is from $g_{a_2 NN}^{(2)} = -1.2$. The data are taken from Ref. [87].

The measurement of the ratio

$$R = \frac{d\sigma/dt(\gamma n \rightarrow \pi^- p)}{d\sigma/dt(\gamma p \rightarrow \pi^+ n)} \quad (54)$$

is of significance to test the validity of the Regge formalism together with the coupling constant and phase chosen for each meson exchange. In Fig. 7 the dominance of the nucleon Born term in both processes leads the ratio to be unity at $-t \approx 0$. The marked minimum just below $-t \approx 0.5$ GeV² may reach by the opposite interference patterns between the $\pm\pi + \rho \pm a_2$ contributions to each other process. It should be noted that the dashed line for the ratio at $E_\gamma = 16$ GeV with $g_{a_2 NN}^{(1)}(g_{a_2 NN}^{(2)}) = 1.4(-1.2)$ is wide out of the data points and, hence, fails to reproduce the measurement. Such numerical evidence supports $g_{a_2 NN}^{(2)} = 0$ as compared to the solid line (red) at the same energy.

2. Spin polarization asymmetries

Single spin polarizations are analyzed for the polarized photon and the target nucleon.

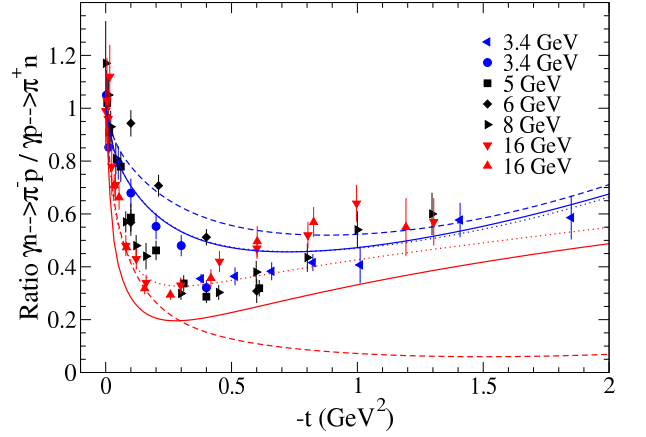


FIG. 7: (Color online) Ratio $R = \frac{d\sigma/dt(\gamma n \rightarrow \pi^- p)}{d\sigma/dt(\gamma p \rightarrow \pi^+ n)}$ at $E_\gamma = 3.4, 5, 6, 8,$ and 16 GeV. Model predictions are given for the two cases $E_\gamma = 3.4$ (upper three blue lines) and 16 GeV (lower three red lines). Solid lines are from the present work with $g_{a_2 NN}^{(1)} = 1.4$ and $g_{a_2 NN}^{(2)} = 0$, while dashed ones are from $g_{a_2 NN}^{(1)} = 1.4$ and $g_{a_2 NN}^{(2)} = -1.2$. Dotted lines are from the GLV model. The result at $E_\gamma = 16$ GeV supports $g_{a_2 NN}^{(2)} = 0$. The data are taken from Refs. [85] (filled squares, filled circles and filled diamonds), [87] (filled left-triangles), [88] (filled down-triangles, filled right-triangles), and [89] (filled up-triangles).

The photon polarization symmetry Σ is defined as

$$\Sigma = \frac{d\sigma_\perp - d\sigma_\parallel}{d\sigma_\perp + d\sigma_\parallel}, \quad (55)$$

where $d\sigma_\perp(d\sigma_\parallel)$ is the differential cross section for the photon polarization along $x(y)$ axis with the z -axis denoted by the direction of the photon propagation in the reaction plane. In terms of the helicity amplitudes [16] the Σ measures the asymmetry between the natural and the unnatural parity exchange so that the contributions of the axial mesons a_1 and b_1 , though negligible for the differential cross section, are to be exposed.

Figure 8 shows the photon polarization Σ in the $\gamma p \rightarrow \pi^+ n$ process with $g_{a_2 NN}^{(2)} = 0$ in accord with the numerical consequence in Fig. 7. The case of $\gamma n \rightarrow \pi^- p$ is presented in Fig. 9 which is further added in proof for $g_{a_2 NN}^{(2)} = 0$, as shown by the numerical consequence at $E_\gamma = 16$ GeV.

In both charged pion processes, the rapid rise of the Σ near threshold is reproduced by the nucleon Born term. Then the Σ is expected to approach to unity by the dominance of the natural parity exchange as the energy increases. It should be stressed that the role of the a_2 exchange is crucial for the better description of the Σ . Without the a_2 exchange our results in the Σ (the dashed lines) are nearly the same as those of the GLV model. We also indicate that our model exhibits the sizable contribution of the axial meson b_1 in these measurements.

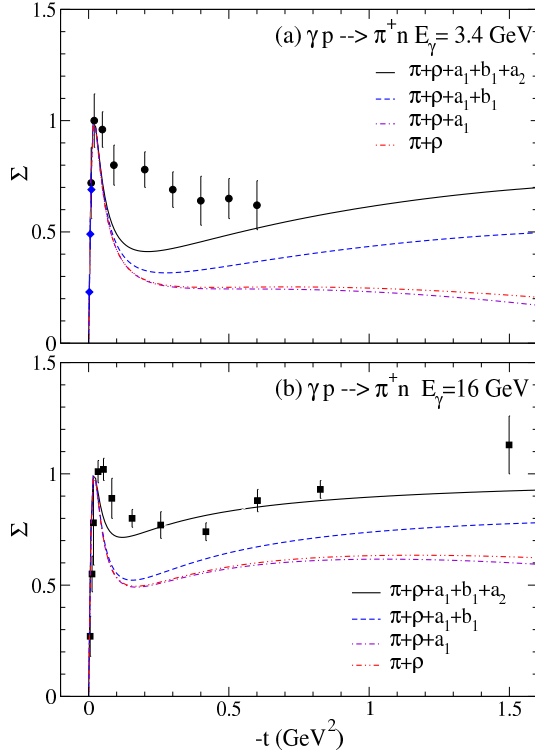


FIG. 8: (Color online) Photon polarization asymmetry for $\gamma p \rightarrow \pi^+ n$ at (a) $E_\gamma = 3.4$ GeV, and (b) $E_\gamma = 16$ GeV. The solid line results from $(\pi + b_1) + a_1 + (\rho + a_2)$ exchanges with $g_{a_2 NN}^{(2)} = 0$. The dashed line is from $(\pi + b_1) + a_1 + \rho$ exchanges. The dash-dotted line is from $\pi + a_1 + \rho$ exchanges. The dash-dot-dotted line is from $\pi + \rho$ exchanges. The data are taken from Refs. [89] (filled squares), [90] (filled diamonds), and [91] (filled circles and filled triangles).

The target polarization asymmetry (T) is defined by

$$T = \frac{d\sigma_{\uparrow} - d\sigma_{\downarrow}}{d\sigma_{\uparrow} + d\sigma_{\downarrow}}, \quad (56)$$

which measures the asymmetry of the spin polarization of the target nucleon parallel and antiparallel to the direction $\frac{\vec{k} \times \vec{q}}{|\vec{k} \times \vec{q}|}$ in the center-of-mass system [93]. With the sharp rise at threshold due to the nucleon Born term, our results exhibit the decisive role of the a_2 exchange in the target polarization, in particular at $E_\gamma = 16$ GeV, as shown in Fig. 10. We note that the results without the a_2 exchange are nearly the same as those of the GLV model calculation (similar to those lines except for the solid one) [17].

B. Neutral pion photoproduction

In the absence of the pion exchange from the neutral case, the dynamics of the production mechanism is solely determined by the exchange of $\omega + \rho^0 + b_1 + h_1$ Regge poles, unless the cuts are considered.

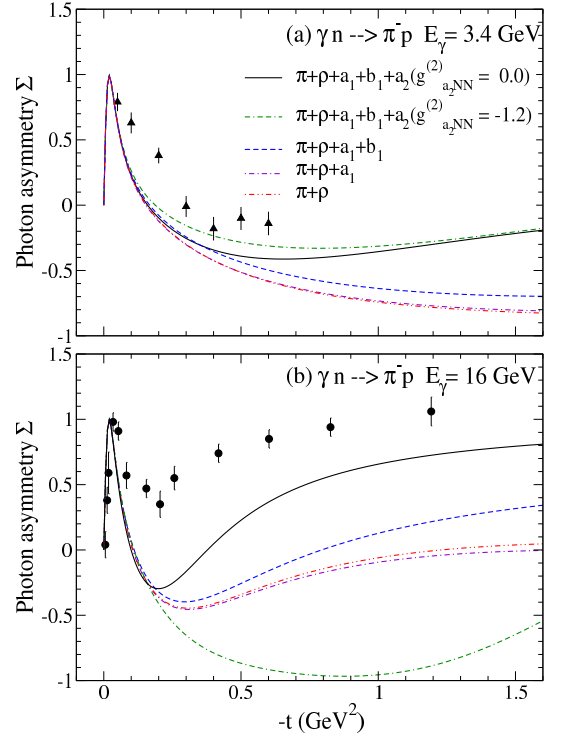


FIG. 9: (Color online) Photon polarization asymmetry for $\gamma n \rightarrow \pi^- p$ at (a) $E_\gamma = 3.4$ GeV (b) $E_\gamma = 16$ GeV. Notations are the same as in Fig. 8. The solid line is from the present model with $g_{a_2 NN}^{(2)} = 0.0$. The dash-dash-dotted line (green) results from $g_{a_2 NN}^{(2)} = -1.2$, showing the failure to reproduce data points at $E_\gamma = 16$ GeV. The data are taken from Refs. [92].

1. Differential cross section and spin polarization asymmetry

The appearance of the deep dip characterizes the feature of the $\gamma p \rightarrow \pi^0 p$ process around $-t \approx 0.5$ GeV² in the differential cross section as well as in the photon polarization. We follow the procedure of Ref. [17] for the dip-generating mechanism by the nonsense wrong signature zero of the dominating Regge trajectory.

In comparison with the coupling strengths between exchanged mesons, the ω exchange would predominate in the process with the large coupling constants for electromagnetic and strong interactions. We, therefore, describe the dip region of the cross section with the nonsense zero of the ω trajectory, i.e., $\alpha_\omega(t) \approx 0$, which occurs precisely at the place the dip is observed in the experiment. We take the phase of the ω exchange to be non-degenerate, $\frac{1}{2}(-1 + e^{-i\pi\alpha_\omega})$, while that of the ρ should be kept degenerate, $e^{-i\pi\alpha_\rho}$, to fill up the singularity of the amplitude at $-t \approx 0.5$ GeV² caused by the nonsense zero value of the α_ω . As an additional dip-filling mechanism, the axial meson exchanges b_1 and h_1 also contribute with the constant phase in common.

The cross sections for the $\gamma p \rightarrow \pi^0 p$ process at $E_\gamma =$

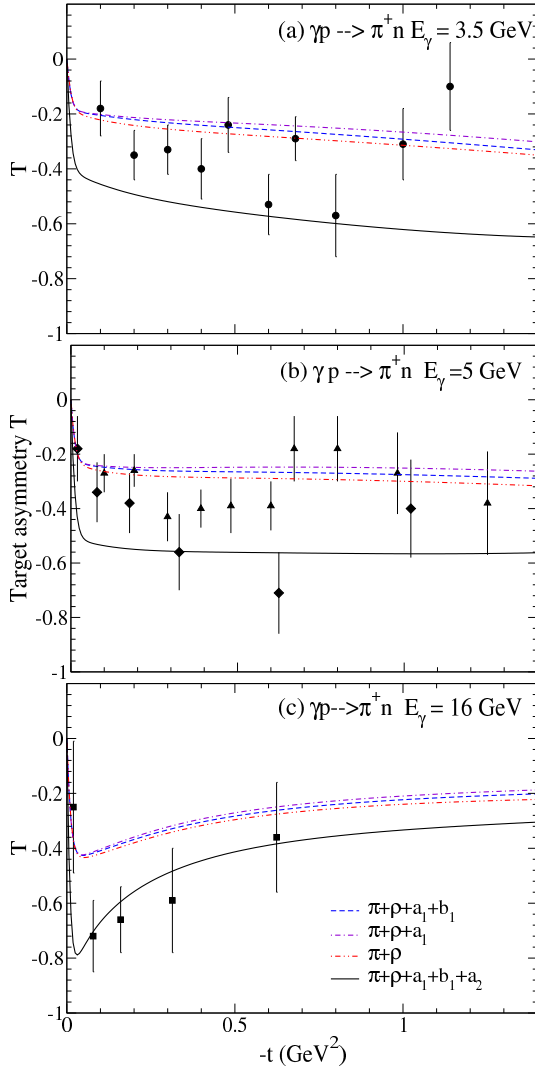


FIG. 10: (Color online) Target polarization asymmetry for $\gamma p \rightarrow \pi^+ n$ at (a) $E_\gamma = 3.4$ GeV, (b) $E_\gamma = 5$ GeV and (c) $E_\gamma = 16$ GeV, respectively in the present work. The solid line results from $(\pi + b_1) + a_1 + (\rho + a_2)$ exchanges with $g_{a_2 NN}^{(2)} = 0$. The data are taken from Ref. [94] (filled circles and filled triangles) and [95] (filled diamonds and filled squares)

6, 9, 12 and 15 GeV are shown in Fig. 11. We find, however, that the $\omega + \rho + b_1 + h_1$ exchanges with the coupling constants in Table IV are in less agreement with the cross section data above the region $-t \approx 0.5$ GeV² as the photon energy increases. Within the context of the present approach where the gross feature of the cross section depends mainly on the singularity of the ω exchange with the leading trajectory α_ω , our model shows deficiency in reproducing the cross section, in particular, over the region $-t \approx 0.5$ GeV² at the higher photon energies, because of the more rapid falloff in the axial meson contributions due to their trajectories lying lower than that of the ω [34].

The ratio for the neutral pion process is presented in

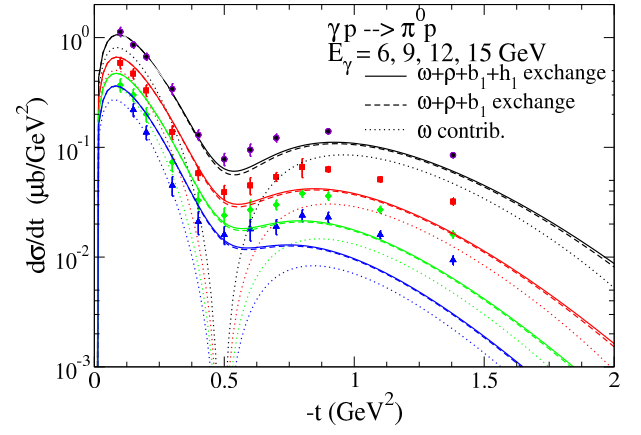


FIG. 11: (Color online) Cross sections for $\gamma p \rightarrow \pi^0 p$ at $E_\gamma = 6, 9, 12, 15$ GeV from the $\omega + \rho + b_1 + h_1$ exchanges in the present model. The data are taken from Ref. [96].

Fig. 12,

$$R = \frac{d\sigma/dt(\gamma n \rightarrow \pi^0 n)}{d\sigma/dt(\gamma p \rightarrow \pi^0 p)}, \quad (57)$$

which shows a slight dip structure in the experimental data. Figure 12 has obtained with all the phases of the Regge poles, ρ , b_1 , and h_1 chosen as constant for the $\gamma n \rightarrow \pi^0 n$ process, while for the $\gamma p \rightarrow \pi^0 p$ process the respective phases of these poles are taken as discussed above. The solid line draws the ratio at $E_\gamma = 4$ GeV. The dashed one at $E_\gamma = 4.7$ GeV and dotted one at $E_\gamma = 8.2$ GeV, respectively. The results are not good enough to explain the data, in particular, over the region $-t \approx 0.5$ GeV². This may reflect the deficiency of the model prediction for the cross section in the region as discussed in Fig. 11. From the isospin symmetry and the negligible role of the axial meson in the cross section, we write the ratio as $R \sim \frac{|\omega - \rho^0|^2}{|\omega + \rho^0|^2}$ symbolically, and expect that the ratio eventually reaches unity by the dominance of the ω , as the data points do at $E_\gamma = 8.2$ GeV.

The photon polarization Σ is presented in Fig. 13. The cross section, the ratio R , and the photon polarization asymmetry Σ for the neutral pion case are sensitive to a change of the phase for the Regge trajectory. Since the Σ measures the asymmetry between the natural and the unnatural exchange, i.e., $\Sigma \simeq \frac{|\omega + \rho^0|^2 - |b_1 + h_1|^2}{|\omega + \rho^0|^2 + |b_1 + h_1|^2}$ written as before, we attempt to modulate the depth of the dip by the contribution of the axial meson negative to the dominating ω exchange and find that the isoscalar h_1 meson plays the role as shown in Fig. 13. It is interesting to see that the h_1 gives much larger contribution than the b_1 . Recall that the solid line (black) is obtained by using the $g_{h_1 NN}^t = -9$ estimated from $\langle q_\perp^2 \rangle \approx 1$ GeV² in Eq. (48) as given in Table IV. But simple guess from the uncertainty principle $\Delta x \Delta q \sim \hbar$ gives much smaller value for the quark momentum squared inside nucleon. The chiral quark model estimate of $\langle q_\perp^2 \rangle = 0.224$ GeV² in Ref. [100], for instance, leads to even the larger values

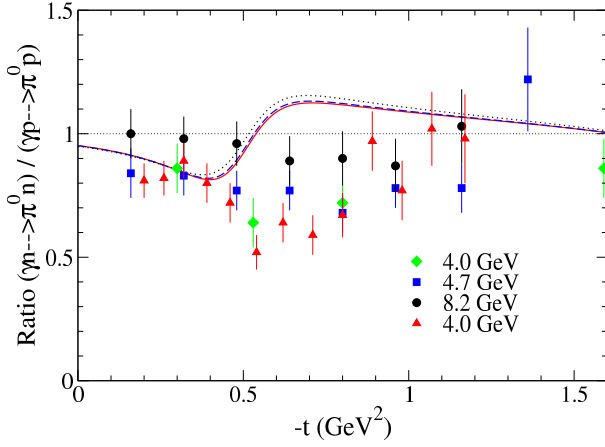


FIG. 12: (Color online) Ratio $R = \frac{d\sigma/dt(\gamma n \rightarrow \pi^0 n)}{d\sigma/dt(\gamma p \rightarrow \pi^0 p)}$ for the differential cross sections. The data are taken from Refs. [97] (filled diamonds), [98] (filled squares, filled circles) and [99] (filled triangles).

for both axial meson coupling constants. The lower solid line (green color) in Fig. 13 shows the case with $g_{h_1 NN}^t = -14$ chosen as much as the b_1 . It is legitimate to point out that the result from the GLV model is not valid for the present case because the vector coupling of the axial meson b_1 they used is not allowed by charge conjugation.

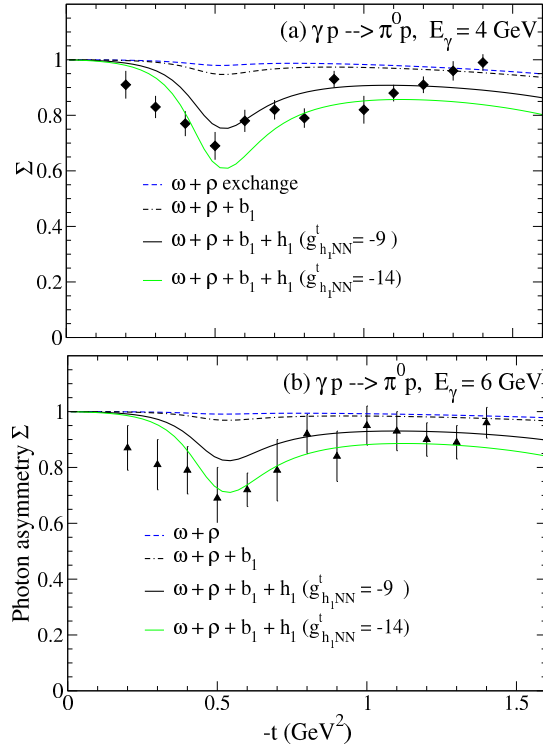


FIG. 13: (Color online) Photon polarization asymmetry for $\gamma p \rightarrow \pi^0 p$ at (a) $E_\gamma = 4$ GeV, (b) $E_\gamma = 6$ GeV. The solid curve results from $\omega + \rho + b_1 + h_1$ exchanges in the present model. The lower solid line (green) results from the change of $g_{h_1 NN}^t = -9$ to -14 . The data are taken from Ref. [96].

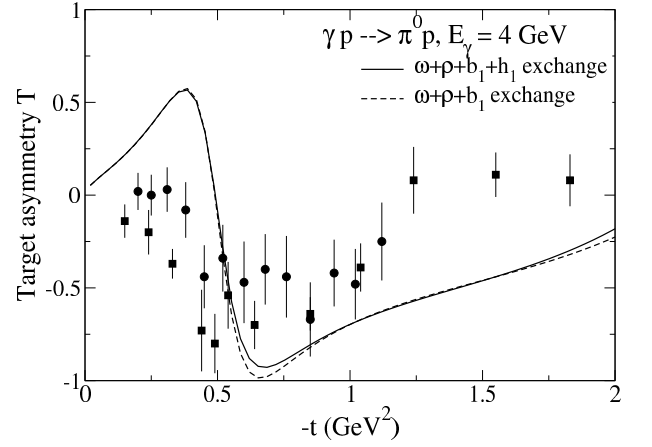


FIG. 14: (Color online) Target polarization asymmetry at $E_\gamma = 4$ GeV in the present work. The data are taken from Refs. [101] (filled squares) and [102] (filled circles).

In Figs. 14 and 15 we show the target and recoil polarization asymmetries at $E_\gamma = 4$ GeV and at $E_\gamma = 6$ GeV, respectively. These observables are by definition related to each other through the model-independent inequality [14],

$$|P - T| \leq 1 - \Sigma, \quad (58)$$

which predicts that they are approximately equal in case of $\Sigma \approx 1$. Indeed, the relation,

$$P - T = 4\pi\sqrt{-t} \text{Im}[f_2^{11} f_2^{01*}], \quad (59)$$

given in terms of the TCHA proves that $P = T$ in the present framework, because the $f_2^{11} = 0$ from the fact that the $\mathcal{A}_3 = 0$ with null contributions of the axial and vector meson exchanges in general, as given in Appendix A. But we need more data in the case of the recoiled polarization to verify the above relation as well as validity of the given model.

We summarize the motivation of the present work and the result we have accomplished here as follows; the present work is initiated by the advantages of the SCHA over the TCHA, which opens the possibility of incorporating the Regge poles in the Born approximation amplitude [16]. This point is worth rephrasing because we thus have an effective theory which enables us to continually work with the Born amplitude from threshold to high energy region in a consistent manner. The theoretical consideration remaining there is an addition of the chiral loop contribution near threshold [1], or the replacement of the fixed- t pole by the Regge pole at high energy [16, 17]. In this sense it is of value to establish the coupling strength of the exchanged particle in an acceptable range of physical values throughout the energy region and, hence, to have the Regge theory basically free of parameters, as we have elaborated on here. To this end we introduce the tensor meson a_2 , and the axial meson h_1 to the existing Regge model of the $\pi + \rho$ exchanges at

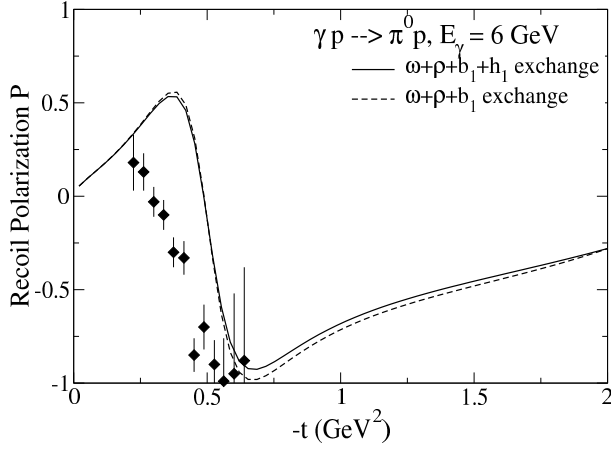


FIG. 15: (Color online) Recoil polarization asymmetry at $E_\gamma = 6$ GeV in the present work. The data are taken from Ref. [103].

the price of its own simplicity. Though not apparent in the present process, it is likely that the difference of the meson-baryon coupling constants between our model and those in Refs. [16, 17] becomes significant in the case of kaon photoproduction. This will be discussed elsewhere.

In the charged pion photoproduction, the inclusion of the a_2 exchange in the primary $\pi + \rho$ + nucleon Born term yields an improved t -dependence of the cross section up to $-t \approx 2$ GeV² as well as the photon polarization. We demonstrate the validity of the coupling constants chosen here by showing the numerical results in better agreement with data. For the neutral case, the exchange of the axial meson h_1 is newly found to give a nontrivial contribution to the photon polarization, while the contribution of the b_1 exchange appears in minor roles.

Acknowledgments

This work was supported by the Korea Research Foundation Grant funded by the Korean Government (KRF-2008-313-C00205).

APPENDIX A

It is worth noting the difference between the TCHA and the SCHA within the Regge formalism. For the two body reaction proceeded via the particle exchange in the t -channel, $1 + 3 \rightarrow 2 + 4$, the Regge pole of a meson exchange in the TCHA is typically given by

$$f_i^{\mu_{13}, \mu_{24}}(s, t) = \beta(t) \frac{1 + \tau e^{-i\pi\alpha(t)}}{\sin \pi\alpha(t)} \left(\frac{s}{s_0} \right)^{\alpha(t)}. \quad (60)$$

The $\beta(t)$ is the factorized residue function with the respective helicity changes denoted by the superscript

$\mu_{ij} = (\mu_i - \mu_j)$. In order to be free of kinematical singularities the residue involves the complicated kinematical t factors, $\alpha(t)$, $(\alpha(t) + 1)$, \dots , to suppress the zeros of $\sin \pi\alpha(t)$ at negative integer values of $\alpha(t)$ [14]. To account for the coupling strengths at the interaction vertices, the residue usually contains some parameters to be fitted to empirical data. Since the residue is not in the form of the vertex coupling usually given by the diagrammatic technique, those parameters are hard to imply the coupling constants in the usual sense.

On the other hand, through crossing of helicity amplitudes $1 + 2 \rightarrow 3 + 4$ for the process in the s -channel exchange, the Regge pole in the SCHA corresponding to Eq. (60) is in general written as [104–106]

$$H_i^{\mu_{34}, \mu_{12}}(s, t) = \left(\frac{-t}{s_0} \right)^{\frac{1}{2}(n+x)} \gamma(t) \frac{1 + \tau e^{-i\pi\alpha(t)}}{2 \sin \pi\alpha(t)} \left(\frac{s}{s_0} \right)^{\alpha(t)} \quad (61)$$

where the $\gamma(t) = \gamma_{13}(t)\gamma_{24}(t)$ is the factorized residue function with the net helicity flip $n = |(\mu_1 - \mu_2) - (\mu_3 - \mu_4)|$. The kinematical t factor in front of the residue comes from the half-angle factors, $\left(\frac{s}{s_0} \frac{1 - \cos \theta}{2} \right) \rightarrow \left(\frac{-t}{s_0} \right)$ and $\left(\frac{1 + \cos \theta}{2} \right) \rightarrow 1$ in the limit $s \gg 4M^2$ and small t [104]. In this case, $(n + x) = |\mu_1 - \mu_3| + |\mu_2 - \mu_4|$ and the factor in power of x is called an evading factor usually neglected for the case of equal masses between the particles. In the SCHA the essential t -singularities are preserved in the half-angle factors, though care must be taken for the evading factor which is introduced by the fact that the Regge pole is a definite parity state in the t -channel with its residue factorizing in terms of t -channel helicities [104].

For the photoproduction with the notation $1(\gamma) + 2(N) \rightarrow 3(\pi) + 4(N)$ above, the reggeized SCHA in Eq. (1) meets with the form in Eq. (61) where the t -singularities correspond to the half-angle factors, and the helicity changes are given by $H_1^{\frac{1}{2}, \frac{3}{2}}, H_2^{\frac{1}{2}, \frac{1}{2}}, H_3^{-\frac{1}{2}, \frac{3}{2}}$, and $H_4^{-\frac{1}{2}, \frac{1}{2}}$ or by $H_1^{(-, -)}, H_2^{(-, +)}, H_3^{(+, -)}$, and $H_4^{(+, +)}$ in terms of the final and initial nucleon helicities in order in the superscript [20].

The TCHA, $f_i^{\mu, \mu'}$, is related to the CGLN-invariant amplitudes [14, 16]. Given explicitly,

$$\begin{aligned} f_1^{01} &= \mathcal{A}_1 - M_+ \mathcal{A}_4, \\ f_2^{01} &= \mathcal{A}_1 + (t - M_-^2) \mathcal{A}_2 - M_- \mathcal{A}_3, \\ f_1^{11} &= M_+ \mathcal{A}_1 - t \mathcal{A}_4, \\ f_2^{11} &= -M_- \mathcal{A}_1 + t \mathcal{A}_3, \end{aligned} \quad (62)$$

and the differential cross section and the photon polarization in this channel are

$$\frac{d\sigma}{dt} = \frac{1}{32\pi} \left[\frac{t|f_1^{01}|^2 - |f_1^{11}|^2}{t - M_+^2} + \frac{t|f_2^{01}|^2 - |f_2^{11}|^2}{t - M_-^2} \right] \quad (63)$$

$$\frac{d\sigma}{dt} \Sigma = \frac{1}{16\pi} \left[\frac{t|f_1^{01}|^2 - |f_1^{11}|^2}{t - M_+^2} - \frac{t|f_2^{01}|^2 - |f_2^{11}|^2}{t - M_-^2} \right] \quad (64)$$

with $M_\pm = (M' \pm M)$ and $M = M'$ in the case of pion photoproduction.

APPENDIX B

Let us now recall the implication of the EXD in the pairs, π - b_1 and ρ - a_2 . To determine the phase of the Regge propagator, this notion together with the G -parity consideration is of importance [11]. In the quark line diagram the $\gamma p \rightarrow \pi^+ n$ process is drawn by the uncrossed channel (planar diagram) for the charge coupling nucleon exchange in the s -channel, whereas the case of $\gamma n \rightarrow \pi^- n$ draws the crossed channel(non-planar) for the u -channel exchange of the charge coupling nucleon. The former diagram leads to a nonzero imaginary part of the amplitude by the optical theorem. In the Regge pole exchange, one possibility for this is to choose the phases of the exchanged mesons in Eq. (19) to be rotating. But the latter diagram leads the production amplitude to a real one, which, then, means that all the phases are taken to be constant in Eq. (20).

According to the finite energy sum rule (which states that the sum of all resonances in low energy is, on the average, approximately equal to the Regge pole at high energy), the dispersion integral for the photoproduction amplitude is given by the sum of the nonresonating background (BG) contribution and the resonance contribution, each of which is related to the Pomeron (P) and the Regge pole, respectively [10],

$$\int_{\nu_0}^{\bar{\nu}} d\nu \nu^n \text{Im } \mathcal{A}_{BG}(\nu, t) = \sum_P \gamma_P(t) \frac{\bar{\nu}^{\alpha_P + n + 1}}{\alpha_P + n + 1}, \quad (65)$$

$$\int_{\nu_0}^{\bar{\nu}} d\nu \nu^n \text{Im } \mathcal{A}_{res}(\nu, t) = \sum_{Regge} \gamma_R(t) \frac{\bar{\nu}^{\alpha_R + n + 1}}{\alpha_R + n + 1} \quad (66)$$

The symmetric variable $\nu = \frac{s-u}{2M}$ and the γ_P and γ_R are the respective residues for the Pomeron and Regge pole exchanges. Since the Pomeron exchange is not allowed for the charged pion case the duality in Eq. (65) is irrelevant. Thus, the optical theorem for the N^* resonances in the $\gamma p \rightarrow \pi^+ n$ process implies that $\text{Im } \mathcal{A}_{res} \neq 0$, so does the sum in the r.h.s. of Eq. (66). This is the case when $\gamma_\pi \neq -\gamma_{b_1}$, and $\gamma_\rho \neq -\gamma_{a_2}$, meaning that the EXD in the pairs, π - b_1 and ρ - a_2 are weak with the phases taken to be imaginary (rotating), but with residues that differ from each other in Eq. (19). For the $\gamma n \rightarrow \pi^- p$ case where the amplitude is real by the quark diagram argument, the $\text{Im } \mathcal{A}_{res}(\nu, t) = 0$ in Eq. (66) implies $\gamma_\pi = -\gamma_{b_1}$, and $\gamma_\rho = -\gamma_{a_2}$, as a consequence. From these duality arguments, we see that the degree of the EXD is stronger in the $\gamma n \rightarrow \pi^- p$ process.

APPENDIX C

The tensor meson dominance (TMD) states that the hadron energy-momentum tensor current $\Theta^{\mu\nu}$ is dominated by the tensor meson $T^{\mu\nu}$. In terms of the source-field identity analogous to the VMD in Eq. (25), this can

be written as [66]

$$\Theta_{\mu\nu} = \frac{m_T^2}{g_T} T_{\mu\nu}, \quad (67)$$

for the source tensor having zero trace as well as zero divergence for brevity. Then, the TMD in the hadron tensor current is manifested by

$$\langle H | \Theta^{\mu\nu}(0) | H \rangle = \frac{\langle 0 | \Theta^{\mu\nu} | T \rangle \langle T, H | H \rangle}{t - m_T^2}, \quad (68)$$

with the $H = \pi$, or N . The application of the TMD to the energy-momentum tensor form factors of the pion, and of the nucleon leads us to the universality of the tensor meson couplings.

Let us now consider the t -channel exchange of the $f_2(1270)$ tensor meson in the πN scattering with the $f_2'(1525)$ assumed decoupled. The interaction Lagrangian is given by

$$\mathcal{L}_{f_2\pi\pi} = \left(\frac{2g_{f_2\pi\pi}}{m_f} \right) \partial_\mu \pi \partial_\nu \pi f_2^{\mu\nu} \quad (69)$$

and the $f_2\pi\pi$ vertex is [67, 74]

$$\langle f_2, \pi | \pi \rangle = \left(\frac{2g_{f_2\pi\pi}}{m_f} \right) 2Q_\mu Q_\nu \epsilon_{(f)}^{\mu\nu} \quad (70)$$

with $Q = \frac{1}{2}(q + q')$. The decay width of $f_2 \rightarrow \pi\pi$ is empirically known and given by

$$\Gamma_{f_2 \rightarrow \pi\pi} = \frac{\alpha}{60\pi} \left(\frac{2g_{f_2\pi\pi}}{m_f} \right)^2 \frac{1}{m_f^2} |k|^5, \quad (71)$$

where $|k| = \frac{1}{2\sqrt{s}} \sqrt{(s - (m + m')^2)(s - (m - m')^2)}$ is the decay momentum and $\alpha=6$ for $f\pi\pi$ and $\alpha=1$ for $a_2 KK$ [30]. From this we estimate $g_{f_2\pi\pi} = 5.9$ from $\Gamma_{f_2 \rightarrow \pi\pi} = 156.9$ MeV and $g_{a_2 KK} = 6.83$ from $\Gamma_{a_2 \rightarrow \pi\pi} = 5.24$ MeV.

The energy-momentum tensor form factor of the pion is defined by

$$\langle \pi(q') | \Theta^{\mu\nu}(0) | \pi(q) \rangle = F_1^\pi(t) (q + q')^\mu (q + q')^\nu, \quad (72)$$

with the condition at $t = 0$,

$$F_1^\pi(0) = \frac{1}{2}, \quad (73)$$

which is determined by the normalization of one pion state with respect to energy [32]. Assume the f_2 -pole dominance, Eq. (68), in the pion form factor in Eq. (72), and use the source-field identity in Eq. (67) for the $\langle 0 | \Theta^{\mu\nu} | f_2 \rangle$ together with the vertex function $\langle f_2, \pi | \pi \rangle$ in Eq. (70) [66],

$$\begin{aligned} & \langle \pi(q') | \Theta^{\mu\nu}(0) | \pi(q) \rangle \\ &= \frac{m_f^2}{g_f} \left(\frac{1}{m_f^2 - t} \right) \left[\frac{g_{f_2\pi\pi}}{m_f} (q + q')^\mu (q + q')^\nu \right], \quad (74) \end{aligned}$$

we obtain

$$F_1^\pi(t) = \frac{m_f}{m_f^2 - t} \frac{g_{f_2\pi\pi}}{g_f}, \quad (75)$$

and at $t = 0$, the universal coupling of f_2 meson is given by

$$g_f = \frac{2g_{f_2\pi\pi}}{m_f} = \frac{11.8}{m_f}. \quad (76)$$

On the other hand, we write the nucleon energy-momentum tensor form factors as

$$\langle N(p') | \Theta^{\mu\nu}(0) | N(p) \rangle = \bar{u}(p') \left\{ \frac{1}{2} F_1(t) (\gamma^\mu P^\nu + \gamma^\nu P^\mu) \right.$$

$$\left. + \frac{F_2(t)}{M} P^\mu P^\nu \right\} u(p), \quad (77)$$

with the following conditions at $t = 0$,

$$F_1(0) + F_2(0) = 1, \quad F_2(0) = 0, \quad (78)$$

which are determined from the normalization of one nucleon state with energy and spin $\frac{1}{2}$. In a similar fashion, the f_2 meson dominance, Eq. (68), in these form factors leads to the following expression,

$$\langle N(p') | \Theta^{\mu\nu}(0) | N(p) \rangle = \frac{m_f^2}{g_f} \left(\frac{1}{m_f^2 - t} \right) \bar{u}(p') \left\{ \frac{2g_{f_2NN}^{(1)}}{M} (\gamma^\mu P^\nu + \gamma^\nu P^\mu) + \frac{4g_{f_2NN}^{(2)}}{M^2} P^\mu P^\nu \right\} u(p), \quad (79)$$

where we use Eq. (51) for the vertex $\langle f_2, N | N \rangle$. Thus, the TMD in the nucleon energy-momentum form factors are given by

$$\begin{aligned} F_1(t) &= \frac{m_f^2}{m_f^2 - t} \frac{4g_{f_2NN}^{(1)}}{g_f M}, \\ F_2(t) &= \frac{m_f^2}{m_f^2 - t} \frac{4g_{f_2NN}^{(2)}}{g_f M}. \end{aligned} \quad (80)$$

Combining the above equations with the conditions, Eq. (78) at $t = 0$, we get the following identities,

$$\frac{2}{M} (g_{f_2NN}^{(1)} + g_{f_2NN}^{(2)}) = \frac{g_{f_2\pi\pi}}{m_f}, \quad g_{f_2NN}^{(2)} = 0, \quad (81)$$

and the universality of coupling constant g_f is given in the form,

$$\frac{4g_{f_2NN}^{(1)}}{M} = g_f = \frac{2g_{f_2\pi\pi}}{m_f}. \quad (82)$$

For the KN scattering we obtain the same identities as in Eq. (81) which relate the $g_{a_2NN}^{(1)}$ and $g_{a_2NN}^{(2)}$ with $g_{a_2K\bar{K}}$ by virtue of the TMD.

-
- [1] V. Bernard, N. Kaiser, and Ulf-G. Meissner, Nucl. Phys. B **383**, 442 (1992).
 - [2] V. K. Magas, E. Oset, and A. Ramos, Phys. Rev. Lett. **95**, 052301 (2005).
 - [3] L. S. Geng, E. Oset, and M. Döring, Eur. Phys. J. A **32**, 201 (2007).
 - [4] I. Zychor *et al.*, Phys. Rev. Lett. **96**, 012002 (2006).
 - [5] M. Fuchs *et al.*, Phys. Lett. B **368**, 20 (1996).
 - [6] K.-H. Glander *et al.*, Eur. Phys. J. A **19**, 251 (2004).
 - [7] J. W. C. McNabb, *et al.*, Phys. Rev. C **69**, 042201(R) (2004); R. Bradford *et al.*, Phys. Rev. C **73**, 035202 (2006).
 - [8] R. G. T. Zegers *et al.*, Phys. Rev. Lett. **91**, 092001 (2003).
 - [9] I. Aznauryan, *et al.*, nucl-th/0907.1901v2.
 - [10] H. Harari, Phys. Rev. Lett. **20**, 1395 (1968).
 - [11] J. K. Storrow, Rep. Prog. Phys. **50**, 1229 (1987).
 - [12] A. C. Irving and R. P. Worden, Phys. Rep. **34**, 117 (1977).
 - [13] B. H. Kellett, Nucl. Phys. B **25**, 205 (1970).
 - [14] A. Sibirtsev, *et al.*, Eur. Phys. J. A **34**, 49 (2007).
 - [15] A. Sibirtsev, *et al.*, Eur. Phys. J. A **41**, 71 (2009).
 - [16] N. Levy, W. Majerotto, and B. J. Read, Nucl. Phys. B **55**, 493 (1973); Nucl. Phys. B **55**, 513 (1973).
 - [17] M. Guidal, J.-M. Laget, and M. Vanderhaeghen, Nucl. Phys. A **627**, 645 (1997).
 - [18] T. Corthals, J. Ryckebusch, T. Van Cauteren, Phys. Rev. C **73**, 045207 (2006).
 - [19] Murat M. Kaskulov and Ulrich Mosel, Phys. Rev. C **81**, 045202 (2010).
 - [20] R. L. Walker, Phys. Rev. **182**, 1729 (1969).
 - [21] G. F. Chew, M. L. Goldberger, F. E. Low, and Y. Nambu, Phys. Rev. **106**, 1345 (1957).
 - [22] M. B. Halpern, Phys. Rev. **160**, 1441 (1967).
 - [23] J. S. Ball, W. R. Frazer and M. Jacob, Phys. Rev. Lett. **20**, 518 (1968).

- [24] J. D. Bjorken and S. D. Drell *Relativistic Quantum Mechanics* (McGraw Hill, New York, 1964).
- [25] Ph. Dennery, Phys. Rev. **124**, 2000 (1961).
- [26] H. Thom, Phys. Rev. **151**, 1322 (1966).
- [27] I. S. Barker, A. Donnachie, and J. K. Storrow, Nucl. Phys. B **95**, 347 (1975).
- [28] R. Worden, Nucl. Phys. B **37**, 253 (1971).
- [29] Byung Geel Yu, Tae Keun Choi and Chueng-Ryong Ji, Phys. Rev. C **70**, 045205 (2004).
- [30] F. Giacosa, Th. Gutsche, V. E. Lyubovitskij, and Amand Faessler, Phys. Rev. D **72**, 114021 (2005).
- [31] H. Kleinert and P. H. Weisz, Lett. Nuo. Cim. **2**, 459 (1971).
- [32] Yong-seok Oh and T.-S. H. Lee, Phys. Rev. C **69**, 025201 (2004).
- [33] V. V. Anisovich and A. V. Sarantsev, hep-ph/0806.1620 (2008).
- [34] A. Donnachie in *Electromagnetic Interactions of Hadrons, Vol. 1*, edited by A. Donnachie and G. Shaw (Plenum, New York, 1978), Vol. 1.
- [35] J. M. Laget, Phys. Rev. C **72**, 022202 (2005).
- [36] H. Nagahiro, L. Roca and E. Oset, Phys. Rev. D **77**, 034017 (2008).
- [37] F. Henyey, Phys. Rev. **170**, 1619 (1968); F. Henyey, G. L. Ksne, Jon Pumplin, and M. H. Ross, Phys. Rev. **182**, 1579 (1969).
- [38] J.-M. Laget, Phys. Lett. B **685**, 146 (2010).
- [39] J.-M. Laget, hep-ph/1004.1949.
- [40] J. J. Sakurai, Phys. Rev. Lett. **22**, 981 (1969).
- [41] J. J. Sakurai, *Currents and Mesons* (University of Chicago Press, Chicago, 1969).
- [42] G. Höhler and E. Pietarinen, Nucl. Phys. B **95**, 210 (1976).
- [43] T. Ericson and W. Weise, *Pions and Nuclei* (Clarendon Press · Oxford, 1988).
- [44] I. Zahed and G. E. Brown, Phys. Rept. **142**, 1 (1986).
- [45] L. Xiong, E. Shuryak, and G. E. Brown, Phys. Rev. D **46**, 3798 (1992).
- [46] K. Haglin, Phys. Rev. D **50**, 1688 (1994).
- [47] C. Amsler *et al.*, Phys. Lett. B **667**, 1 (2008).
- [48] M. Zielinski *et al.*, Phys. Rev. Lett. **52**, 1195 (1984).
- [49] Particle Data Group, Eur. Phys. J. C **3**, (1998).
- [50] M. Birkel and H. Fritzsche, Phys. Rev. D **53**, 6195 (1996).
- [51] L. Gamberg and G. R. Goldstein, Phys. Rev. Lett. **87**, 242001 (2001); hep-ph/0106178.
- [52] M. Gari and U. Kaulfuss, Phys. Lett. B **138**, 29 (1984).
- [53] J. W. Durso and G. E. Brown, Nucl. Phys. A **430**, 653 (1984).
- [54] R. L. Jaffe and Xiangdong Ji, Phys. Rev. Lett. **67**, 552 (1991).
- [55] J. Soffer, Phys. Rev. Lett. **74**, 1292 (1995).
- [56] H. He and X. Ji, Phys. Rev. D **52**, 2960 (1995); **54**, 6897 (1996).
- [57] H.-C. Kim, M. Polyakov, and G. Goeke, Phys. Rev. D **53**, R4715 (1996).
- [58] S. Aoki, M. Doui, T. Hatsuda and Y. Kuramashi, Phys. Rev. D **56**, 433 (1997).
- [59] R. L. Jaffe and X. Ji, Nucl. Phys. B **375**, 527 (1992).
- [60] K. Suzuki and T. Shigetani, Nucl. Phys. A **626**, 886 (1997).
- [61] M. Wakamatsu and T. Kubota, Phys. Rev. D **60**, 034020 (1999).
- [62] R. Alkofer, H. Reinhardt and H. Weigel, Phys. Rep. **265**, 139 (1996).
- [63] L. Gamberg, H. Weigel and H. Reinhardt, Phys. Rev. D **58**, 054014 (1998).
- [64] I. Schmidt and J. Soffer, Phys. Lett. B **407**, 331 (1997).
- [65] V. Barone, A. Drago and P. G. Ratcliffe, Phys. Rept. **359**, 1 (2002).
- [66] K. Raman, Phys. Rev. D **2**, 1577 (1970); Phys. Rev. D **3**, 2900 (1971).
- [67] B. Renner, Phys. Lett. B **33**, 599 (1970).
- [68] J. Engels, Nucl. Phys. B **25**, 141 (1970).
- [69] J. Baacke, T. H. Chang and H. Kleinert, Nuo. Cim. A **12**, 21 (1972).
- [70] P. Carruthers, Phys. Rev. D **2**, 2265 (1970).
- [71] M. Suzuki, Phys. Rev. D **47**, 1043 (1993).
- [72] V. Barger, M. Olsson, and K. V. L. Sarma, Phys. Rev. **147**, 1115 (1966).
- [73] David J. Gross and Heinz Pagels, Phys. Rev. **172**, 1381 (1968).
- [74] H. Goldberg, Phys. Rev. **171**, 1485 (1968).
- [75] E. Borie and F. Kaiser, Nucl. Phys. B **126**, 173 (1977).
- [76] P. M. M. Maessen, Th. A. Rijken, and J. J. de Swart, Phys. Rev. C **40**, 2226 (1989).
- [77] M. M. Nagels, T. A. Rijken, and J. J. de Swart, Phys. Rev. D **17**, 768 (1978).
- [78] V. G. J. Stoks and Th. A. Rijken, Phys. Rev. C **59**, 3009 (1999).
- [79] V. G. J. Stoks and Th. A. Rijken, Nucl. Phys. A **613**, 311 (1997).
- [80] M. M. Nagels, T. A. Rijken, and J. J. de Swart, Phys. Rev. D **12**, 744 (1975).
- [81] M. M. Nagels, T. A. Rijken, and J. J. de Swart, Phys. Rev. D **15**, 2547 (1977).
- [82] Th. A. Rijken and Y. Yamamoto, Phys. Rev. C **73**, 044008 (2006).
- [83] V. G. J. Stoks and Th. A. Rijken, Phys. Rev. C **59**, 3009 (1999).
- [84] Th. A. Rijken, V. G. J. Stoks, and Y. Yamamoto, Phys. Rev. C **59**, 21 (1999).
- [85] P. Heide *et al.*, Phys. Rev. Lett. **21**, 248 (1968).
- [86] P. M. Joseph *et al.*, Phys. Rev. Lett. **19**, 1206 (1967).
- [87] Z. Bar-Yam *et al.*, Phys. Rev. Lett. **19**, 40 (1967).
- [88] A. M. Boyarski *et al.*, Phys. Rev. Lett. **20**, 300 (1968).
- [89] D. J. Sherden *et al.*, Phys. Rev. Lett. **30**, 1230 (1973).
- [90] H. Burfeindt, *et al.*, Phys. Lett. B **33**, 509 (1970).
- [91] C. Geweniger, *et al.*, Phys. Lett. B **29**, 41 (1969).
- [92] H. Burfeindt, *et al.*, Nucl. Phys. B **59**, 87 (1973);
- [93] Byung Geel Yu, Tae Keun Choi and Chueng-Ryong Ji, J. Phys. G **32**, 387 (2006).
- [94] H. Genzel, *et al.*, Nucl. Phys. B **92**, 196 (1975);
- [95] Charles C. Morehouse, *et al.*, Phys. Rev. Lett. **25**, 835 (1970)
- [96] R. L. Anderson, *et al.*, Phys. Rev. D **4**, 1937 (1971)
- [97] G. C. Bolon *et al.*, Phys. Rev. Lett. **27**, 964 (1971).
- [98] A.M. Osborne, *et al.*, Phys. Rev. Lett. **29**, 1621 (1972).
- [99] W. Braunschweig, *et al.*, Nucl. Phys. B **51**, 157 (1973);
- [100] M. Wakamatsu, Phys. Rev. D **79**, 094028 (2009).
- [101] P. S. L. Booth, *et al.*, Phys. Lett. B **38**, 339 (1972).
- [102] H. Bienenlein, *et al.*, Phys. Lett. B **46**, 131 (1973).
- [103] M. Deutsch, *et al.*, Phys. Rev. Lett. **29**, 1752 (1972).
- [104] P. D. B. Collins, *An Introduction to Regge Theory & High Energy Physics* (Cambridge University press, Cambridge, 1977).
- [105] G. Cohen-Tannoudji, P. Salin, and A. Morel, Nuo. Cim. **55A**, 412 (1968).
- [106] M. Le Bellac, Nuo. Cim. **55A**, 318 (1968).